Manuscript Details

Manuscript number	IJRMMS_2018_1176_R1
Title	Failure mechanisms and stability analyses of granitic boulders focusing a case study in Galicia (Spain)
Article type	Research paper

Abstract

Granitic boulders are widespread geomorphological elements, particularly found in humid granitic areas. Although they seldom represent a hazard for people or infrastructures, sometimes their location in steep or natural slopes may jeopardise their stability and potentially affect people or infrastructures. In addition, their complex geometry makes the instability mechanisms difficult to identify, so it is even more difficult to compute factors of safety regarding their stability. In this paper, the authors analyse potential failure mechanisms of granite boulders based on analytical mechanic calculations and physical tilt tests, permitting understanding the phenomena under scrutiny. Then, they study the stability of one of these boulders: the Pena do Equilibrio or equilibrium rock. To do that they resort to standard geotechnical characterization and advanced geometrical characterization derived from UAV photogrammetric and 3D Laser Scanning of the boulder. The presented results exemplify how the application of these recently available topographic technologies, in combination with rock mechanics approaches, enable a rigorous analysis of the stability of granite boulders.

Keywords	boulder; geomorphology; basic friction angle; stability; 3D printing
Taxonomy	Rock Mechanics, Geomorphological Aspects
Corresponding Author	Ignacio Pérez-Rey
Corresponding Author's Institution	University of Vigo
Order of Authors	Ignacio Pérez-Rey, Leandro R. Alejano, Adrian Riquelme, Luis Miguel González de Santos

Submission Files Included in this PDF

File Name [File Type]

IJRMMS_2018_1176_cover_letter.docx [Cover Letter]

IJRMMS-2018-1176-response-to-reviewers-and-editor.docx [Response to Reviewers]

highlights_perez_rey_et_al_2018_ijrmms.docx [Abstract]

perez_rey_et_al_2018_ijrmms_REV_VERSION-28-march.docx [Manuscript File]

Fig_1.tif [Figure]

Fig_2.tif [Figure]

Fig_3.tif [Figure]

Fig_4.tif [Figure]

Fig_5.tif [Figure]

Fig_6.tif [Figure]

Fig_7.tif [Figure]

Fig_8.tif [Figure]

Fig_9.tif [Figure]

Fig_10.tif [Figure]

Fig_11.tif [Figure]

Fig_12.tif [Figure]

Fig_13.tif [Figure]

Fig_14.tif [Figure]

Fig_15.tif [Figure]

Table_1.docx [Table]

Table_2.docx [Table]

Table_3.docx [Table]

Table_4.docx [Table]

Submission Files Not Included in this PDF

File Name [File Type]

video_1.mp4 [Video]

video_2.mp4 [Video]

To view all the submission files, including those not included in the PDF, click on the manuscript title on your EVISE Homepage, then click 'Download zip file'.

Failure mechanisms and stability analyses of granitic boulders focusing a case study in Galicia (Spain)

I. Pérez-Rey[1], L.R. Alejano[1], A. Riquelme[2], L. González[1]

[1]Department of Natural Resources and Environmental Engineering, University of Vigo. Campus Universitario Lagoas-Marcosende, s/n, 36310 Vigo (Spain)

[2]Department of Civil Engineering, University of Alicante. Carr. San Vicente del Raspeig, 03690 San Vicente del Raspeig, Alicante (Spain)

Abstract

Granitic boulders are widespread geomorphological elements, particularly found in humid granitic areas. Although they seldom represent a hazard for people or infrastructures, sometimes their location in steep or natural slopes may jeopardise their stability and potentially affect people or infrastructures. In addition, their complex geometry makes the instability mechanisms difficult to identify, so it is even more difficult to compute factors of safety regarding their stability. In this paper, the authors analyse potential failure mechanisms of granite boulders based on analytical mechanic calculations and physical tilt tests, permitting understanding the phenomena under scrutiny. Then, they study the stability of one of these boulders: the *Pena do Equilibrio* or equilibrium rock. To do that they resort to standard geotechnical characterization and advanced geometrical characterization derived from UAV photogrammetric and 3D Laser Scanning of the boulder. The presented results exemplify how the application of these recently available topographic technologies, in combination with rock mechanics approaches, enable a rigorous analysis of the stability of granite boulders.

Keywords: boulder; geomorphology; basic friction angle; stability; 3D printing

Corresponding author: I. Pérez-Rey (iperez@uvigo.es)

1. Introduction

Large granite boulders are distinctive geomorphological elements or structures usually found in mountain or abrupt granitic humid areas. A large amount of rainfall contributes to the processes eventually leading to the formation of these boulders, so they tend to be more common in wet temperate climates. Therefore, these granite boulders are common all over the world, but particularly in regions such as northern Spain[1,2], Portugal[3,4], Italy[5], Turkey[6], USA[7–9], Southern Australia[10,11], Brazil[12], Hong-Kong[13] or Malaysia[14]. Occasionally, the instability of these boulders represent a potential hazard for people or infrastructures[1,15].

These boulders are formed through evolving spheroidal weathering[16,17] so they tend to present a roughly spheroidal or ellipsoidal shape, but in practice they often show surface irregularities associated with the heterogeneous nature of granitic rock and with the occurrence of pre-existing rock mass discontinuities that partially control their formation.

Traditional rock slope engineering studies[18,19] developed methodologies to analyse the stability of geometrical shaped rock blocks delimited by pre-existing planar discontinuities, such as rock slabs, prisms, wedges or columns. These potentially unstable blocks tend to form when excavating engineered slopes or rock cuts. Stability against sliding or toppling of individual or sets of these elements can be quantified according to these approaches.

However, methodologies to estimate the stability of naturally occurring granite boulders of irregular shape have not been developed so far, something the authors attribute to two facts. Firstly, rarely does the stability of boulders involve a hazard for people or infrastructures; secondly, the complex geometry of these boulders was difficult to measure and their stability cannot be easily quantified according to existing approaches.

Nevertheless, some studies on the stability of individual or sets of boulders can be found in literature. In this way, Christianson et al.[15] analysed the stability of some Buddha carvings in granite boulders in Japan accounting for potential seismic triggering effects; Alejano et al.[1] presented a stability analysis of a boulder in a study that partially motivated the development of the current work. Moreover, some authors of this manuscript studied the stability against toppling of rock slabs with rounded corners, first on an individual basis[20] and then for the case of a number of interacting rock slabs in line with the block toppling stability analysis proposed by Goodman and Bray[21], for the case of sharp-edge

and rounded-edge blocks[22]. Undoubtedly, a typical granite boulder is nothing but a cubic or slab-shaped rather irregular granite block subjected to spheroidal weathering. So the approaches developed in the mentioned publications have also served as an input for the development of the present study.

Even though the actual majority of these boulders is not usually hazardous, if the block is located in a cliff or a natural slope, it may fall down. This potential rock-fall of unstable boulders has shown to cause accidents and being of concern in a number of places reflected in the literature[23,24]. In this sense, it is interesting to develop approaches to quantify its stability. Additionally, analysing the stability of granitic boulders could contribute to a better understanding of geodynamical evolution, not only for granitic but also for other rock masses.

Based on these two mentioned reasons, the authors consider of interest to develop a rock mechanics approach to quantify boulder stability. Within this framework, we present in this paper a stability study of a paradigmatic granitic boulder —*Pena do Equilibrio* ('equilibrium stone')— located in Galicia (NW Spain). To do that, the authors have first resorted to advanced surveying techniques in order to obtain a detailed geometry of the boulder, and to rock characterisation methods to estimate the friction of the rock contact surface. Then, and based on physical modelling of engineered small-size blocks, we have reviewed techniques to estimate factors of safety against sliding and toppling for different shapes and positions of irregular blocks. Finally, we have extended physical models and calculations to quantify the stability of the granitic boulder under scrutiny, and the obtained results made sense in relation to actual stability observations, also agreeing reasonably well with a 3D-printed physical model of the boulder.

The presented approach can be extended or adapted to quantify the stability of other cases involving irregularly-shaped granitic boulders.

2. Geomorphological context

Boulders can be considered one of the most common and characteristic landforms of granitic terrains[25]. Their origin can be encountered within the typical weathering sequence of granitic rock masses, a process described by Durgin[26], in which four typical stages can be recognised: fresh rock, corestones, decomposed granitoid and saprolite. The development of these structures is dominated by the mechanism of spheroidal weathering,

a chemical process that mainly affects uniform, well-jointed rocks like granite, dolerite or basalt, but also other lithologies such as gabbros and sandstones[16].

The process of boulder formation is developed in two stages: first, subsurface differential-weathering acts on the granitic rock mass, being complemented afterwards with erosive events (wind, rainfall), which develop the eventual excavation of the corestone to form a boulder (**Fig. 1**). Subsurface weathering principally alters micas and feldspars to produce clays, with the intervention of different chemical processes such as solution, alteration and hydrolysis[25].

Weathering of granitic batholiths presents joint-controlled geomorphic features, which means that it is clearly dependent on the rock mass structure, particularly on their main joint sets, usually displayed orthogonally. Fracturing spacing is considered the main factor affecting maximum size and shape of boulders, whereas roundness and the actual size depend on the duration and intensity of subsurface weathering[17].

In general terms, boulders appear in different shapes, from almost perfect spheres to ellipsoidal bodies and even slender slabs, depending not only on the weathering degree to which they were subjected, but also on the geometrical variability of the joint sets affecting the granitic rock mass. Migoń[17] has related the presence of isolated or clustered huge boulders to coarse-grained, potassium-rich, post-kinematic (post-Variscan) granites, whereas boulder fields, with sizes rarely exceeding 2 m long, have been associated to much older fine-grained granitic areas. Some examples showing geometrical and size diversity of boulders are illustrated in **Fig.** 2 Weights range from 1 to 10,000 tons and all pictures are taken in the NW corner of the Iberian Peninsula, including the regions of Galicia in Spain and Minho in Portugal.

3. Understanding stability of boulders

On some occasions, granitic boulders can be encountered either isolated or clustered but displayed as balanced rocks, that's to say, potentially close to a limit-equilibrium state (**Figs. 2d** and **2g**). This fact may imply an instability hazard, incremented by the huge size reached by some of these structures —i.e. *The Leviathan* boulder[25], with an approximate length of 33 m— but, essentially, due to their possible location at spots presenting steep slopes. These features could eventually lead to instability, and sometimes subsequently to a rockfall event, representing a threat for any structure or population located in the falling path.

Some works focusing on the study of these structures have been mostly carried out in the field of geomorphology[25,27] and applied paleoseismology[28,29]. There barely exists any contribution, regarding stability of boulders, from a rock mechanics standpoint. Moreover, some of these studies have focused on the stability of slender blocks[20,30], some of them from a rock slope engineering perspective and mainly revisiting toppling mechanisms[22,31–33]. Other authors have analyzed the maximum boulder size forming in overhanging cliffs associated to tensile failure and the occurrence of earthquakes, but the failure mechanisms analyzed differed from the case of rounded granite boulders under study here [34,35]. Due to all these particularities, it has been considered important to provide tools for correctly assessing the stability of potentially unstable boulders.

In the heart of this study, it has been observed that the main instability mechanisms affecting boulders lying on slopes —sliding and toppling— could be relevantly affected by some geometrical features, like the actual shape of the boulder, mass distribution and the type of contact between the boulder and the resting surface. In this line, some approaches, by means of simple engineered rock and 3D printed elements, have been carried out aiming to understand the effect of these factors on block stability. These analyses also served to develop a realistic approach for estimating the stability state of a balanced granitic boulder.

3.1. Laboratory physical modelling of simple geometric models

With the aim of studying the stability of the *Pena do Equilibrio* boulder, it was considered relevant to review first the traditional procedure for estimating safety factor, particularly for toppling failure (considering gravity as the unique driving force), in order to be applied later to the boulder under scrutiny. To test the analytical approach and analyse factors at stake, some rock models with symmetric and asymmetric sections were selected and engineered in laboratory by cutting and assembling smaller granitic pieces (**Fig. 3a-g**). The advantage of these physical models resides in their simple basic geometry, which allows a simple analytical estimation of the angle of toppling for each specimen. Additionally, it is possible to carry out simple tilt tests under controlled environmental conditions and constant lifting velocities (12 °/min), analysing, in an experimental manner, the analytically predicted angles (against toppling or sliding).

The stability against sliding is controlled by the plane dip (β) and the basic friction angle of the used granite (Eq. 1) which was found to be 31±2º in a large series of tilt tests[36].

$$FoS_{sliding} = \frac{\tan \phi_b}{\tan \beta} \quad (1)$$

The basic equation controlling the stability against toppling of a rigid block is presented in Eq. 2 and it can be used to estimate the factor of safety, and subsequently, the stability of a block against toppling. This simple equation just considers the ratio of the stabilizing and overturning moments, which in the simplest case where the only driving force is the weight of the specimen can be computed according to the forces acting along x and y-axes, in relation to a rotation axis located in the lower corner of the block in the direction of tilting.

$$FoS_{toppling} = \frac{\sum M_{stabilising}}{\sum M_{overturning}} \quad (2)$$

The forces involved in the analysis of each specimen result only from its own weight and they are applied at the centres of gravity of the specimens, in the case of symmetric figures (i.e. **Fig. 3h**, specimen 4) or at the centres of gravity of subsections, in the case of the rest of asymmetric figures (**Fig. 3i**). The most prone mechanism: sliding or toppling, will be the one theoretically occurring at a lower tilting angle.

Eq. 3 shows the application of Eq. 2 to analyse stability against toppling of specimen 1 presented **Fig. 3i**, considering the indicated rotation axis.

$$FoS_{toppling,1} = \frac{W_1\left(\frac{a}{2}+\frac{a}{4}\right)cos\beta + W_2\frac{a}{4}cos\beta + W_3\frac{a}{3}cos\beta}{W_1 a sin\beta + W_2\frac{a}{4}sin\beta + W_3\frac{4a}{3}sin\beta} \quad (3)$$

Specimens with 4 potential bases represented as 1 and 3 in **Fig. 3h** were tested at 8 different positions (as depicted in **Fig. 4** for the case of specimen 1), carrying out 3 tilt tests for each scenario; specimen 2 was only tested at 6 positions due to its geometry. Specimens 4, 5 and 6 were tested in 2 positions in only one base. In all the cases, the corresponding stability calculations based on Eq. 1 and 2, as the example shown in Eq. 3 were performed and a theoretical prediction of the failure mechanisms and angle of sliding or toppling was theoretically estimated. An example of results and tilting instability angles for theoretical calculations for specimen 1 is illustrated in **Fig. 4.**

188 The instability mechanism observed in the lab (sliding or toppling) was registered as
189 well as the inclination at which it happens. All angles were measured with an inclinometer
190 *Leica DISTO D5*, with an accuracy of 0.1° for all series. Results were reflected in Table
191 1.
192 The effect of a curved contact on the stability of rounded or cylindrical specimens
193 has been also studied by means of analytical and laboratory physical modelling (**Fig. 5a**).
194 This was made for evaluating the influence that a concave contact may have on the
195 stability of actual boulders. To assess this in laboratory, a 3D printer —model *BCN Sigma*
196 *3D* (**Fig. 5b**)— has been used to create two plastic bases presenting a circular concave
197 surface with different contact depths (r/3 and r/6) being r = 27.25 cm; this radius
198 corresponds to a NX Brazilian-test specimen, as shown in **Fig. 5c**.
199 For the two cases (r/3 and r/6), the angle of toppling was first analytically estimated
200 by means of Eq. 2 (**Fig. 5d**). Then, three tilt tests were carried out under the same
201 conditions as the other specimens, by employing the two plastic implements and by
202 registering the angles of overturning. It has been demonstrated again the good correlation
203 between results coming from theoretical calculations and from laboratory tests and it has
204 also been observed the relevant effect of base concavity on stability: for the studied
205 radius, r = 27.25 mm, if the contact depth is incremented from r/6 to r/3, then the angle
206 of toppling will change from 33.6° to 48.2°, which would enhance stability in about 40%.
207 **Fig. 6** shows those points representative of the theoretical (x-axis) and experimental
208 (y-axis) angles of failure against sliding (represented by crosses) and toppling
209 (represented by dots) for all tested specimens. As it can be appreciated, the dataset
210 correlates quite well with the 1:1 line, yielding a Pearson's correlation coefficient, r =
211 0.994. This indicates that the analytical framework proposed for estimating the angle of
212 failure can be considered appropriate for the case of all these tested specimens.
213 All results obtained from tilt tests together with those estimated through the
214 application of Eq. 1 and 2 are presented in **Table 1** for all specimens and testing positions.
215 In this table, error is simply the difference between analytical and experimental angles. It
216 is relevant to remark that the average value of errors from all results in **Table 1** is -0.3º
217 with a standard deviation of 1.3º, an indication that for controlled geometry and surface
218 strength our stability computing capacity is rather accurate. However, it should be pointed
219 out that all these samples have a constant granite thickness (they have a vertical symmetry
220 plane, containing their gravity centre, whose projection for the horizontal position falls in
221 the centre of the base); and for tilting they are positioned with the symmetry plane normal

222 to the strike of the tilting surface. This makes calculations simpler. For the case of
223 irregular boulders resting on rock planes, this may not always be the case, so stability
224 computations may not be that straight forward.

225 Based on in-situ observation of some irregular boulders and, in particular, of the case
226 under scrutiny, it is necessary to be able to analyse the stability in case, for the solid under
227 study resting on a horizontal plane, the projection of its centre of gravity does not fall in
228 the centre of its base and the rotating axis is not a straight line parallel to the strike of the
229 tilting plane.

230 To study this scenario in laboratory, it was carried out a tilt test involving two
231 cylindrical specimens with same radius, r = 27 mm (one made up of a gneiss with
232 approximate density ρ_r = 2700 kg/m^3 measuring 100 mm-height and the other one made
233 up of steel, with approximate density ρ_s = 7800 kg/m^3 and measuring 35 mm-height).
234 This test consisted in placing the two specimens in the way shown by **Fig. 7a**, that is with
235 the top piece moved outwards a distance r/2. This position of the top steel specimen
236 distances the centre of gravity out of the plane of symmetry of the lower specimen, as it
237 can be appreciated in the front view **Fig. 7b**. Then, the specimen was progressively tilted
238 until toppling of the entire set occurred, when the tilting angle was registered. The
239 experiment was also repeated with both specimens aligned by their vertical axis.

240 From the whole experiment, two observations (which may be of relevance when
241 assessing the stability of real boulders) can be extracted. Firstly, for a given tilting angle
242 (β) the safety factor is reduced with respect to those configurations which keep the centre
243 of gravity in a symmetry plane (e.g. tilt test with both specimens aligned); secondly, the
244 rotation point, for the not-aligned set, becomes deviated from the line of maximum slope,
245 as shown by δ angle in **Fig. 7b**.

246 Based on this test configuration (**Fig. 7a**) with the top specimen displaced, it is
247 possible to obtain, first, the factor of safety (Eq. 4) at any moment in the tilting process
248 and also the slope β_{crit} at which the set will be unstable (Eq. 5). Additionally, in this case,
249 the element does not topple in the direction of maximum slope but in a direction forming
250 an angle δ with this one, which can be computed as proposed by Eq. 6.

251 $$FoS = \frac{M_{stab.}}{M_{overt.}} = \frac{W \cdot x_{G-crit} \cos\beta}{W \cdot z_G \sin\beta} = \frac{x_{G-crit}}{x_G} = \frac{\tan\beta_{crit}}{\tan\beta} \quad (4)$$

252 $$\beta_{crit.} = \tan^{-1}\frac{x_{G-crit}}{z_G} \quad (5)$$

$$\delta = \tan^{-1} \frac{y_G}{x_{G-crit}} \quad (6)$$

Some detailed calculations for this test are presented in **Fig. 7** where from angles of $\beta_{crit} = 17.3^{o}$ and $\delta = 14.2^{o}$ were obtained, consistent with the results observed in the tilt tests. The authors have carried out three repetitions of tests for the case of the steel piece offset r/2 in both directions and for the case with the sample centred. Results are presented in the last lines of **Table 1** showing good agreement. The 1° difference between the analytical and experimental results can be attributed to a small rounding in the base of the gneiss specimen. In addition, the fact of not toppling in the maximum slope direction was observed by justifying the computed δ angle. A video of this test is enclosed within the Additional Material.

3.2. Effect of rounding on the stability of boulders

The rounding of block edges and corners represent the evident effect of the spheroidal weathering mechanism affecting rock masses. From an engineering point of view, this effect may have relevant influence on the stability of slender rock slabs against toppling, but also in actual rock slopes prone to fail under this mechanism, as studied by Alejano et al.[20,22]. The basic influence of a rounded edge associated to the rotating axis can be quantified according to the equations illustrated in **Fig. 8**. Readers are referred to the above-mentioned references for further analysis. Regarding the role played by the spheroidal weathering mechanism on the development of granitic boulders, the effect of rounding has been found relevant when analysing stability particularly against toppling, but it may also affect sliding slightly.

To gain insight on these effects and based on the presented equations (**Fig. 8**), a 2D rectangular block of length, L; height, H and circular rounding of the edges, with the (circular) radius of curvature denoted as r_c, has been analysed in terms of stability against toppling failure. The effect of rounding is introduced in the following analysis by a *roundness factor*, ρ, defined as the ratio of the radius of curvature of the corners (r_c) over a length equal to half base of the block (L/2). In this way, $\rho = 0$ corresponds to a slab with sharp edges and $\rho = 1$ regards a block with a semi-circular base which will tend to topple even when vertically standing in a horizontal plane.

Based on this rounding factor, it is possible to create a chart providing dip angles corresponding to instability as illustrated in **Fig. 9.** For different values of the roundness

285 factor and contact plane dip angles, different curves for the factor of safety considering
286 various L/H ratios are provided. **Fig. 9** shows that sub-vertical ellipsoidal boulders are
287 more prone to instability than the spheroidal ones and being this spheroidal one more
288 prone to instability than sub-horizontal ellipsoidal ones. Indicatively, if we take a value
289 of ρ = 0.5, where we have rounded edges of half of the length of the block, the plump
290 blocks (L/H = 2.7) will be stable when resting on a plane less than 53º dip (around 70º
291 for edged blocks), the squared ones (L/H=1) for less than 27º (45º for no rounding) and
292 the slender ones (L/H = 0.5) for less than 15º (27º for no rounding). In conclusion, it is
293 clear that rounding plays a key role in instability and that this role can be quantified for
294 perfectly rounded corners.
295

296 ## 4. The case of *Pena do Equilibrio* boulder.

297 The granitic boulder under scrutiny, locally known as *Pena do Equilibrio*
298 ('Equilibrium Stone'), is located near the town of Ponteareas in the province of
299 Pontevedra (Galicia, NW Spain). Geologically, the rock that forms the boulder has been
300 described by the Spanish Geological Survey (IGME)[37] as a fine-to-medium-grained,
301 biotite-amphibole granodiorite. The structure lies over a granitic base, standing some
302 meters above a road, and forming a sort of granitic plinth, as can it be observed in **Fig.**
303 **10**.

304 Some features of this boulder have motivated the assessment of its stability, being the
305 obvious one the risk perception. Other particularities are a pseudo-ellipsoidal geometry
306 and rather large dimensions (about 9 m length and 3.7 m height), the position above a
307 local road and the natural inclination, β, with which it is displayed respect to the ground
308 (approximately $\beta = 27°$ dip). Another relevant feature is the small contact area between
309 the boulder and the base.
310

311 ### 4.1. 3D surveying and geometrical calculations

312 Regarding the complex shape of the boulder and its small contact area, the first step
313 to perform stability analyses required a painstaking in-situ 3D surveying of the structure.
314 The use of a Terrestrial Laser Scanner (TLR) was successfully applied to determine the
315 geometry of geological structures by 3D point-cloud acquisition, in particular of rock
316 boulders[27]. This technique was selected to perform the topographical survey of the

boulder under study, specifically those parts demanding high accuracy, like the contact area. To perform this task, a *FARO Focus 330X LiDAR* was selected. Several scan stations were performed to scan all the boulder surface, and the data were registered using external targets. A 3D point cloud (3DPC) was generated in a local reference system. All scan stations were levelled, being the vertical axis of the local reference system (z-axis) coincident with the gravity direction. Consequently, dip measurements can be directly extracted from the 3DPC. In addition to the external targets, several targets were placed on the base of the boulder and consequently scanned. The local coordinates of these targets were extracted for further application of the boulder reconstruction. Special attention was paid to the scanning of the boulder-base contact.

The situation and size of the boulder prevented a complete terrestrial scanning, specifically of the upper face. Therefore, the TLS survey was complemented with aerial imagery obtained with a 12 Mpx camera mounted on a *Phantom 3* Unmanned Aircraft System (UAS). **Fig. 11** shows different aerial photographs, which were eventually processed and exported as a 3DPC by means of the photogrammetric suite *Photoscan*[38]. The Structure from Motion (SfM) reconstruction process included the previously located targets on the base of the boulder. Coordinates of these targets were inserted as Ground Control Points (GPC's) and the SfM reconstruction was registered to the TLS 3DPC (i.e., both 3DPC were defined in the same local reference system). Finally, both 3DPC's merged into one, providing very accurate information of the entire area. Once the complete 3DPC was processed, it was necessary to isolate the boulder from the general dataset (**Fig. 12 a, b**), a task carried out with the software *CloudCompare*[39]. The contact area was calculated by creating a 3D polyline at the contour corresponding to the intersection between those points of the boulder and those of the lower rock where it rests. The 3D polyline was afterwards projected onto a plane, giving a contact surface of approximately 0.61 m^2 (**Fig. 12c**).

The estimation of volume and centre of mass of the boulder required the generation of a mesh, by using Poisson surface reconstruction[40], from the SfM-TLS merged 3DPC. This process was carried out with the open software *MeshLab*[41]. For the given mesh, the estimated volume was 142.22 m^3 and the centre of gravity is located at local coordinates x = 7.914 [m], y = -2.851[m], z = 113.036 [m], being z-axes coincident with gravity direction.

Table 2 summarises some geometrical parameters of the boulder under study, which were useful to carry out stability analyses against sliding and toppling.

4.2. Geomechanical characterization of the contact

A basic geomechanical characterization was carried out in order to obtain information regarding parameters needed to quantify stability. This included density and basic rock joint characterization according to the Barton strength criteria[42–44]. Rock samples were collected and cut into slab-like specimens, which were tested for density and for the basic friction angle (ϕ_b). The average density obtained was 2.57 g/cm^3, and the median of ϕ_b, for five tests, was 34º with a standard deviation of 1º, obtained from tilt tests run according to an ISRM Suggested Method[45].

The surfaces of the studied boulder and the block where this one rests, were characterized around the contact area. Schmidt hammer rebound tests were made on the surface near the contact and in fresh rock; roughness profiles were measured with the help of a Barton's comb. The following values of basic parameters were obtained, as presented in **Table 3**.

4.3. Stability assessment of the *Pena do Equilibrio* boulder

4.3.1. Assessment of sliding failure

The assessment of stability against sliding failure for the present case has been carried out by following planar failure analysis with an extension of Eq. 1 adapted for the case under study. Although it was initially thought to estimate shear strength of the contact based on the approach proposed by Barton and Bandis[42] considering scale effects of rough unfilled rock joints, this approach was discarded. Although the contact between the two blocks was originally a fresh joint, in the process of weathering associated to the boulder formation, the contact joint has suffered alteration. Shear strength is obviously dependent on the joint surface geometry that, for the case under study, has been subjected to continuing modifications by in situ physicochemical processes, such as weathering and alteration, and even shearing and rock crushing[46].

It has been largely observed that the so-called Barton-Bandis[42] approach works reasonably well for natural joints with matching sides. Nevertheless, this technique cannot be directly applied to rock block contacts, where joint sides do not match, as each side has a different *JRC* and shear behaviour tends to be more dependent on the contact area than on the side *JRC*.

To overcome this problem, Zhao[47] proposed a new version of Barton's formula named the *JRC-JMC* shear strength model. This strength criterion takes into account the additional influence of the so-called joint matching coefficient (*JMC*) a parameter to be estimated, based on the matching of the two joint sides.

$$\tau_{Zhao} = \sigma_n \tan\left[\phi_r + JMC\ JRC_n \log_{10}\left(\frac{JCS_n}{\sigma_n}\right)\right] \quad (7)$$

This is a variation of the Barton-Bandis formula where the *JMC* parameter has to be included. Some studies have shown that this parameter depends on the level of contact of the surfaces. Based on an estimation of potential contact of the surface, on previous experiences developed by the authors on large granite block tilt testing[48] and on the recommendation by Zhao[47] the *JMC* should be equalled to 0.3; when any value lower than this is estimated, *JMC* was set to this value (*JMC*=0.3) for the studied contact.

In order to compute stability, first, the weight of the boulder (W_b) was estimated. Based on the volume recovered from the 3D point cloud (**Table 2**) and considering the average specific weight of the rock, γ_{rock} = 25.7 kN/m^3, the weight of the boulder was estimated in 3655 kN. Therefore, theoretical normal and shear stresses exerted by the boulder at the contact plane, as depicted in **Fig. 13**, for a dip angle β = 27°, become (Eq. 8 and 9):

$$\sigma_{n,b} = \frac{W_b \cos\beta}{A} \cong 5.34\left[\text{MPa}\right] \quad (8)$$

$$\tau_b = \frac{W_b \sin\beta}{A} \cong 2.72\left[\text{MPa}\right] \quad (9)$$

Shear strength, τ_a, available at the contact was computed by means of Eq. 7[47], considering the following in-situ estimative inputs for the equation:

- Basic friction angle, ϕ_b = 34°
- Number of Schimdt-hammer rebounds for the contact plane, r = 46, so JCS = 112 MPa
- Number of Schmidt-hammer rebounds for a fresh rock surface, R = 52
- Joint matching coefficient, JMC = 0.3
- Joint Roughness Coefficient, JRC = 11
- Residual friction angle, $\phi_r = (\phi_b - 20°) + 20(r/R)$ = 31.7°
- L_n = 0.9 (length of contact, as recovered from the 3DPC); so, according to Barton and Bandis[42]: JRC_n = 6.8 and JCS_n = 54.3 MPa

The results show an estimated peak friction angle of 33.7º and a shear strength, τ_a, available at the contact of 3.56 MPa. The safety factor against sliding (FoS_s) can be computed from Eq. 8, for two scenarios: the first one without considering the seismic effect (FoS_s), representative of the actual state of the boulder and the second one ($FoS_{s,\alpha}$), by taking into account a pseudo-seismic analysis where the effect of the maximum seismic coefficient expected for Spanish design standards is used[49] (α = 0.032). The seismic effect is accounted for by considering the corresponding horizontal acceleration applied in the direction of the maximum slope:

$$FoS_{s,\alpha} = \frac{\left(W_b \cos\beta - \alpha W_b \sin\beta\right)\tan\phi_{peak}}{W_b \sin\beta + \alpha W_b \cos\beta} \quad (10)$$

Therefore, the safety factor without considering the seismic effects becomes $FoS_{s,a}$ = 1.31; when a seismic design approach is considered (α = 0.032), the safety factor is reduced to $FoS_{s,\alpha}$ = 1.21. α refers to the seismic acceleration for stability analysis and it is the ratio between the maximum expected horizontal acceleration and gravity, which should be applied in the center of gravity of the potentially unstable solids to account for the effect of earthquakes in the area. This indicates that the boulder is reasonably stable against sliding, even under the worst possible expectable circumstances. Inputting a combination of the most negative geomechanical values to obtain the lowest possible FoS, the computed values for the standard case and according to seismic act will become 1.16 and 1.07 respectively so, still stable. We can conclude that the *Pena do Equilibrio* boulder is stable against sliding under foreseeable circumstances.

4.3.2. Assessment of toppling failure

Toppling failure represents one of the most widespread types of instability affecting rock slopes. The safety factor against toppling failure can be studied for the boulder under scrutiny, by taking into account the position of its actual centre of gravity with respect to the contact plane and following the approach illustrated in Section 3.1 and **Fig. 13**. The fact that the normal projection of the centre of gravity is outside the contact base, indicates that if the contact plane had been horizontal, the boulder would toppled backwards.

Taking advantage of the precise 3D point cloud available for the area under study, it is possible to fit a plane —by using the tool *FitPlane* included in the software *CloudCompare*[39]— to the 3D polyline presented in Section 5.1.3. This plane will be representative of the contact area between the boulder and the rock mass where it rests.

In this line, it is possible to obtain from the software the coefficients A = 0.12689, B = –0.44511, C = 0.88643 and D = –100.5267, which correspond to the general equation of this mentioned plane (π), as shown by Eq. 11:

$$\pi = Ax + By + Cz + D = 0.12689x - 0.44511y + 0.88643z - 100.5267 = 0 \quad (11)$$

Since the centre of gravity (*cog*) of the boulder is represented by a point in the space (three coordinates, as presented in **Table 2**), it is thus possible to obtain the orthogonal distance (point-plane distance, *d*) between this point and the contact area. Given the point $P_{cog}(x_0, y_0, z_0)$ = (7.915, –2.854, 113.036) representative of the *cog*, the normal distance from the plane to that point is estimated, with Eq. 12, as Z_{CG} = 1.95 m.

$$d\left(P_{cog}, \pi\right) = Z_{CG} = \frac{\left|Ax_0 + By_0 + Cz_0 + D\right|}{\left(A^2 + B^2 + C^2\right)^{1/2}} \quad (12)$$

If the *cog* and normal component of the weight of the boulder ($W_b \cos\alpha$)' are projected onto a horizontal plane (**Fig. 14**), a simple estimation of the factor of safety against toppling can be computed. This can be carried out by relating the actual dip of the contact plane (β = 27°) with the critical angle of toppling (β_{crit} = 31.4°), similarly estimated as by Eq. 2.

Therefore, the safety factor against toppling for the presented boulder under study becomes (Eq. 13):

$$FoS_t = \frac{\tan\beta_{crit.}}{\tan\beta} = \frac{\tan 31.4^{\circ}}{\tan 27^{\circ}} \cong 1.20 \quad (13)$$

If the maximum expected seismic coefficient in the area α = 0.032 is taken into account, then, FoS will go down to 1.11.

Computation of the angle called δ in a similar way as in Section 3.2, will yield a value of approximately 20.5º, indicating that the boulder will topple not along the maximum slope line, but in a direction forming an angle δ with this line towards the position of the centre of gravity of the boulder.

In parallel with all these presented calculations, a polylactide (PLA) plastic replica of the actual boulder under study was engineered by means of a 3D printer, *BCN Sigma 3D* (**Fig. 15 a-c**). Once obtained the volumetric mesh corresponding to the original boulder, it was resized to an approximate 1:50-scale, with the help of the freeware *BCN3D Cura*[50].

In the replica, a piece of sandblast paper was fixed on the base of the block representing the location of the contact area, with the aim of avoiding sliding through that contact. The contact does not represent the shear strength properties of the actual contact

476 in the boulder; however, the geometry of the plastic boulder can represent the overturning
477 proneness of the rock boulder.
478 This replica was subjected to a series of tilt tests, as those performed for the rock
479 pieces presented in Section 3.1 in order to analyse the angle at which toppling occurs.
480 Five tilt tests were carried out in the way shown by **Fig. 15d**. As it can be checked, results
481 presented in **Table 4** (with a mean value of 30.4°) are in line with the critical angle of
482 toppling, $\beta_{crit.}$ = 31.4°, as previously presented. It is relevant to remark that in all tilt tests
483 the toppling of the boulder occurred in a direction (δ = 20°) slightly divergent of that of
484 maximum slope, in line with the angle computed (a video with one of these tests is
485 provided within the Additional Material).
486

487 ### 4.3.3. Stability in the event of a large earthquake

488 It has been shown that the factors of safety against sliding and toppling of the boulder
489 were computed in 1.31 and 1.20, respectively. These values diminish to 1.20 and 1.11
490 when considering a horizontal acceleration $\alpha = 0.032 \cdot g$, as recommended by the Spanish
491 seismic protection act[49].
492 These factors of safety were also computed for a different scenario, as that
493 experienced on the area under study during the occurrence of an extraordinary
494 earthquake, with epicentre in the SW Portuguese margin in 1755[51], the so-called Lisbon
495 earthquake. According to Amaré-Tafalla et al.[52], the effects of this mega-seism, could be
496 quantified in grade VII for the MKS intensity scale[53] in the municipality where the
497 boulder locates. The maximum coefficient for seismic acceleration α could be roughly
498 estimated as α = 0.065 for these conditions[54]. Accounting for this horizontal acceleration,
499 the corresponding factors of safety will become $FoS_{s,\ \alpha = 0.065}$ = 1.12 and $FoS_{t,\ \alpha = 0.065}$ =
500 1.03.
501 Human beings genetically evolved to identify risk. The perception of every person
502 visiting the stone is that it may fall, so the stone is name 'Equilibrium Stone'. This should
503 mean that this boulder is not far from equilibrium, something that the above numbers
504 seem to confirm.
505

5. Discussion

Granitic boulders, typical of humid regions, are often odd-shaped rounded-corner blocks, so analysis of their stability may become a non-straight-forward task. A number of physical model tilt tests performed in small rock elements of various shapes have help to illustrate some issues regarding stability calculations of these blocks in relation to sliding and toppling phenomena. For instance, rock elements with asymmetric geometry, concave contacts and rounded-corners were tested.

Based on the study and calculations presented, rather accurate stability estimates of these odd-shaped blocks can be derived, at least, at the same level of those related to more typical failures in rock slope engineering such as planar or wedge failure.

For the case of toppling instability, the most relevant aspect to be accounted for is the geometry of the boulder and the location of the rotation point in its base in relation to the boulder's center of gravity. Since advanced techniques can compute very accurately boulder geometry, results are deemed to be reliable. The occurrence of a convex or concave surface in the base of the boulder may slightly affect results, but information on this surface tends to be hidden, so some uncertainty in this regard can be expected.

For the case of sliding instability, the strength response of the contact zone is the most significant issue impacting stability. Since this contact cannot be considered a standard rock joint but a contact between two rock pieces the reliability of strength is difficult to quantify. Previous empirical tests by the authors[46] on this type contacts for the case of smaller blocks (around 50 kg and around 2 tons) would indicate standard deviations in friction angles around 2 to 3º.

The fact that the granite boulders have irregular complex geometrical forms have made difficult to reliably compute their stability in the past. Application of Terrestrial Laser Scanner in combination with UAS photogrammetric techniques permits nowadays obtaining a very accurate and comprehensive geometrical representation of these boulders. This in turn, in combination with point cloud management software provides accurate positioning of the centre of gravity of the boulder and the contact zones.

A good knowledge of the topography of the boulder, including the shape and nature of its contact base, together with an appropriate characterization of its base as a mismatched rock discontinuity, allows carrying out reliable stability computation of boulder under different environmental circumstances, including earthquakes. In particular, an accurate geometry representation is critical to analyse stability against the toppling of boulders. This approach may contribute to better understanding of a number

of phenomena so far difficult to quantify in the field of engineering geology and risk assessment. The use of plastic replicas available from 3D printing can be helpful to contribute to stability studies based on physical modelling, even if inherent printout heterogeneity as well as rounded contact edges could lead to slight differences between analytic and physical model results.

6. Conclusions

An ellipsoidal granitic boulder of about 142 m^3 and 380 t is located in the province of Pontevedra (Galicia, Northwest Spain). Some particularities like its location on the side of a slope, a somewhat small contact area and the natural inclination with which it is displayed have motivated the study of the stability against slide and toppling failure.

Some laboratory tilt testing was carried out aiming to revisit traditional stability equations by employing rock physical models. Taking advantage of 3D printing techniques it has been studied the effect of particular geometrical aspects —like a circular contact area— on the stability of blocks against toppling. As a result of this, the equation for calculating a safety factor for toppling can be validated and adapted for irregular rock elements with non-planar contact surfaces.

Advanced remote-sensing techniques, such as terrestrial LiDAR and aerial imagery, have been successfully applied, in order to obtain an exact geometry either of the actual contact area and boulder under study. These techniques facilitated the stability analyses, carried out by means of traditional computation, both for sliding and toppling mechanisms under different scenarios. In this line, the management of the recovered 3D point clouds allowed a reasonable positioning of the forces and momentum involved as well as having available good estimations of the contact area and volume of the boulder.

As a general conclusion, the current stability condition of the boulder can be assured both for sliding and toppling with safety factors of 1.31 and 1.20, respectively. In case of accounting for seismic acceleration in line with Spanish seismic standard ($\alpha = 0.032$) this factors of safety will become 1.20 and 1.11 respectively so the boulder would still be stable. If an extremely unexpected event occurs, like an earthquake increasing the seismic acceleration to $\alpha = 0.065$, the stability of the boulder might be compromised.

The presented approach may serve as a guideline for further studies on granite boulder stability, or for other natural rock slope stability phenomena associated with the occurrence of irregular rock elements.

References

1. Alejano LR, Ordóñez C, Armesto J, Rivas T. Assessment of the instability hazard of a granite boulder. *Nat Hazards*. 2010;53(1):77-95. doi:10.1007/s11069-009-9413-0.
2. Ayala-Carcedo FJ, Cubillo-Nielsen S, Alvarez A, et al. Large scale rockfall reach susceptibility maps in La Cabrera Sierra (Madrid) performed with GIS and dynamic analysis at 1:5,000. *Nat Hazards*. 2003;30(3):325-340. doi:10.1023/B:NHAZ.0000007095.12516.90.
3. Vidal-Romaní J. Granite geomorphology in Galicia (NW Spain). *Cad do Lab Xeolóxico Laxe Rev Xeol galega e do hercínico Penins*. 1989;13:89-163.
4. Migoń P, Vieira G. Granite geomorphology and its geological controls, Serra da Estrela, Portugal. *Geomorphology*. 2014;226:1-14. doi:https://doi.org/10.1016/j.geomorph.2014.07.027.
5. Pera E Le, Sorriso-Valvo M. Weathering and morphogenesis in a mediterranean climate, Calabria, Italy. *Geomorphology*. 2000;34(3):251-270. doi:https://doi.org/10.1016/S0169-555X(00)00012-X.
6. Aydin A. Stability of saprolitic slopes: nature and role of field scale heterogeneities. *Nat Hazards Earth Syst Sci*. 2006;6(1):89-96. doi:10.5194/nhess-6-89-2006.
7. Tolman C, Robertson F. *Exposed Precambrian Rocks in Southeast Missouri*. Missouri Division of Geological Survey and Water Resources Report of Investigations (no. 44); 1969.
8. Fisher T. River Warren boulders, Minnesota, USA: catastrophic paleoflow indicators in the southern spillway of glacial Lake Agassiz. *Boreas*. 2004;33(4):349-358. doi:10.1111/j.1502-3885.2004.tb01245.x.
9. Chapin CE, Kelley SA, Cather SM. The Rocky Mountain Front, southwestern USA. *Geosphere*. 2014;10(5):1043-1060. http://dx.doi.org/10.1130/GES01003.1.
10. Twidale C. *Granite Landforms*. Elsevier; 1982.
11. Twidale C. The antiquity of the Australian landscape. *Cad do Lab Xeolóxico Laxe Rev Xeol galega e do hercínico Penins*. 1989;13:7-30.
12. Valeriano C, Magalhães A. Geologia estrutural da área do Pão de Açucar e adjacências, Rio de Janeiro, Brasil. *An Acad Bras Cienc*. 1984;56(3):295-301.
13. GEO. *Geotechnical Engineering Office. Guide to Site Investigation (Geoguide 2)*. Hong Kong: The Government of the Hong Kong Special Administrative Region;

607 2017.
608 14. Md Dan MF, Muhamad ET, Komoo I, Alel MNA. Physical characteristics of
609 boulders formed in the tropically weathered granite. *J Teknol*. 2015;72(3):75-82.
610 doi:10.11113/jt.v72.4015.
611 15. Christianson M, Itoh J, Nakaya S. Seismic analysis of the 25 Stone Buddhas Group
612 at Hakone, Japan. *35th US Symp Rock Mech*. 1995:6. https://doi.org/.
613 16. Ollier CD. Causes of spheroidal weathering. *Earth-Science Rev*. 1971;7(3):127-
614 141. doi:https://doi.org/10.1016/0012-8252(71)90005-5.
615 17. Migoń P. *Geomorphological Landscapes of the World: 2. Granite Landscapes of*
616 *the World*. Oxford University Press; 2006.
617 18. Hoek E, Bray J. *Rock Slope Engineering*. Chapman & Hall; 1974.
618 19. Wyllie D, Mah C. *Rock Slope Engineering*. 4th ed. CRC Press (Taylor and Francis
619 Group); 2004.
620 20. Alejano LR, Carranza-Torres C, Giani G, Arzúa J. Study of the stability against
621 toppling of rock blocks with rounded edges based on analytical and experimental
622 approaches. *Eng Geol*. 2015;195:172-184. doi:10.1016/j.enggeo.2015.05.030.
623 21. Goodman R, Bray J. Toppling of rock slopes. In: *Proceedings of the Specialty*
624 *Conference on Rock Engineering for Foundations and Slopes. Vol. 2*. ; 1976.
625 22. Alejano LR, Sánchez-Alonso C, Pérez-Rey I, et al. Block toppling stability in the
626 case of rock blocks with rounded edges. *Eng Geol*. 2018;234.
627 doi:10.1016/j.enggeo.2018.01.010.
628 23. de Almeida JA, Kullberg JC. Rockfall hazard and risk analysis for Monte da Lua,
629 Sintra, Portugal. *Nat Hazards*. 2011;58(1):289-310. doi:10.1007/s11069-010-
630 9668-5.
631 24. Topal T, Akin MK, Akin M. Rockfall hazard analysis for an historical Castle in
632 Kastamonu (Turkey). *Nat Hazards*. 2012;62(2):255-274. doi:10.1007/s11069-
633 011-9995-1.
634 25. Twidale C, Vidal-Romaní J. *Landforms and Geology of Granite Terrains*. CRC
635 Press (Taylor and Francis Group); 2005.
636 26. Durgin P. Landslides and weathering of granitic rocks. In: Coates D, ed. *Reviews*
637 *in Engineering Geology: Landslides*. Boulder, Colorado: The Geological Society
638 of America; 1977:278. doi:https://doi.org/10.1130/REG3.
639 27. Armesto J, Ordóñez C, Alejano LR, Arias P. Terrestrial laser scanning used to
640 determine the geometry of a granite boulder for stability analysis purposes.

Geomorphology. 2009;106(3):271-277. doi:https://doi.org/10.1016/j.geomorph.2008.11.005.

28. Brune JN, Bell JW, Anooshehpoor A. Precariously balanced rocks and seismic risk. *Endeavour*. 1996;20(4):168-172. doi:https://doi.org/10.1016/S0160-9327(96)10029-6.

29. Purvance MD, Anooshehpoor A, Brune JN. Freestanding block overturning fragilities: Numerical simulation and experimental validation. *Earthq Eng Struct Dyn*. 2009;37(5):791-808. doi:10.1002/eqe.789.

30. Purvance MD. *Overturning of Slender Blocks: Numerical Investigation and Application to Precariously Balanced Rocks in Southern California (PhD Dissertation)*.; 2009.

31. Liu CH, Jaksa MB, Meyers AG. Toppling mechanisms of rock slopes considering stabilization from the underlying rock mass. *Int J Rock Mech Min Sci*. 2010;47(2):348-354. doi:10.1016/j.ijrmms.2009.11.008.

32. Bobet A. Analytical solutions for toppling failure. *Int J Rock Mech Min Sci*. 1999;36(7):971-980.

33. Yagoda-Biran G, Hatzor YH. A new failure mode chart for toppling and sliding with consideration of earthquake inertia force. *Int J Rock Mech Min Sci*. 2013;64:122-131. doi:10.1016/j.ijrmms.2013.08.035.

34. Siman-Tov S, Katz O, Matmon A. Examining the effects of ground motion and rock strength on the size of boulders falling from an overhanging cliff. *Eng Geol*. 2017;220:164-174. doi:10.1016/J.ENGGEO.2017.02.008.

35. Katz O, Reichenbach P, Guzzetti F. Rock fall hazard along the railway corridor to Jerusalem, Israel, in the Soreq and Refaim valleys. *Nat Hazards*. 2011;56(3):649-665. doi:10.1007/s11069-010-9580-z.

36. Alejano LR, Muralha J, Ulusay R, et al. A Benchmark Experiment to Assess Factors Affecting Tilt Test Results for Sawcut Rock Surfaces. *Rock Mech Rock Eng*. 2017;50(9). doi:10.1007/s00603-017-1271-6.

37. IGME. Geological Map of Spain: sheet 224 (Puenteareas). *MAGNA 50k (2nd Ser*. 1981.

38. Agisoft. Agisoft Photoscan Professional. 2018. http://www.agisoft.com.

39. Girardeau-Montaut D. CloudCompare. 2018.

40. Kazhdan M, Bolitho M, Hoppe H. Poisson Surface Reconstruction. In: Polthier K, Sheffer A, eds. *Eurographics Symposium on Geometry Processing*. The

675 Eurographics Association; 2006.
676 41. Cignoni P, Callieri M, Corsini M, Dellepiane M, Ganovelli F, Ranzuglia G.
677 MeshLab: an Open-Source Mesh Processing Tool. In: Scarano V, Chiara R De,
678 Erra U, eds. *Eurographics Italian Chapter Conference*. The Eurographics
679 Association; 2008.
680 doi:10.2312/LocalChapterEvents/ItalChap/ItalianChapConf2008/129-136.
681 42. Barton N, Bandis S. Effects of block size on the the shear behaviour of jointed
682 rock. In: *The 23rd U.S Symposium on Rock Mechanics (USRMS)*. Berkeley,
683 California: American Rock Mechanics Association; 1982.
684 43. Barton N, Choubey V. The shear strength of rock joints in theory and practice.
685 *Rock Mech*. 1977;10(1):1-54. doi:10.1007/BF01261801.
686 44. Barton N. Review of a new shear-strength criterion for rock joints. *Eng Geol*.
687 1973;7(4):287-332. doi:https://doi.org/10.1016/0013-7952(73)90013-6.
688 45. Alejano LR, Muralha J, Ulusay R, et al. ISRM Suggested Method for Determining
689 the Basic Friction Angle of Planar Rock Surfaces by Means of Tilt Tests. *Rock*
690 *Mech Rock Eng*. October 2018. doi:10.1007/s00603-018-1627-6.
691 46. Zhao J. Joint surface matching and shear strength part A: joint matching coefficient
692 (JMC). *Int J Rock Mech Min Sci*. 1997;34(2):173-178. doi:10.1016/S0148-
693 9062(96)00062-9.
694 47. Zhao J. Joint surface matching and shear strength. Part B: JRC-JMC shear strength
695 criterion. *Int J rock Mech Min Sci Geomech Abstr*. 1997;34(2):179-185.
696 doi:10.1016/S0148-9062(96)00063-0.
697 48. Alejano LR, Veiga M, Gómez-Márquez I, Taboada J. Stability of granite drystone
698 masonry retaining walls: II. Relevant parameters and analytical and numerical
699 studies of real walls. *Géotechnique*. 2012;62(11):1027-1040.
700 doi:10.1680/geot.10.P.113.
701 49. MFOM. Real Decreto 997/2002, de 27 de septiembre, por el que se aprueba la
702 norma de construcción sismorresistente: parte general y edificación (NCSR-02).
703 *Boletín Of del Estado*. 2002;244:35898-35967.
704 50. BCN3D. BCN3D Cura. 2018.
705 51. Baptista MA, Miranda JM. Revision of the Portuguese catalog of tsunamis. *Nat*
706 *Hazards Earth Syst Sci*. 2009;9(1):25-42. doi:10.5194/nhess-9-25-2009.
707 52. Amaré Tafalla M, Orche García E, Puche Riart O. Efectos del terremoto de Lisboa
708 de 1 de noviembre de 1755 en la antigua provincia de Tuy (Galicia) - The effects

of Lisbon earthquake of 1 november, 1755 on the Ancient Province of Tuy. *Cuad Dieciochistas*. 2005;6:117-152.

53. Medvedev S V, Sponheuer W. Scale of seismic intensity. In: *IV World Conference on Earthquake Engineering*. Santiago (Chile); 1969:143-152.

54. Brady AG, Trifunac MD. On the correlation of seismic intensity scales with the peaks of recorded strong ground motion. *Bull Seismol Soc Am*. 1975;65(1):139-162. https://doi.org/.

743 **FIGURE CAPTIONS**

744

745 **Figure 1** (a) Sketch showing the development of boulders as a consequence of the two-
746 stage process by the spheroidal weathering mechanism; (b) Incipient spheroidal
747 weathering observed in a granitic outcrop (Sanxenxo, NW Spain).

748

749 **Figure 2**. Different examples of granitic boulders in the NW Iberian peninsula: (a)
750 ellipsoidal boulder still surrounded by highly decomposed granite; (b) quasi-spherical
751 boulder recently released from completely decomposed granite; (c) boulder presenting a
752 sub-vertical crack; (d) ellipsoidal rocking stone, something attributed to a concave base;
753 (e) twin boulders; (f) large boulder probably fallen down from a close mountain; (g) very
754 large boulder (10,000 tons) in a mountain peak and (g) slab-like rounded cornered blocks.
755 Location of every boulder written below every picture and approximate scale reflected.
756 All pictures by authors.

757

758 **Figure 3** (a)-(g) Rock specimens used for the experimental program to review safety
759 factor equation; (h) Sketch of the specimens used for the experimental determination of
760 the angle of toppling; (i) Sketch of the subdivision of one specimen for estimating factor
761 of safety against toppling, including the location of the centres of gravity of its parts.

762

763 **Figure 4** Example of sketches of the eight-type tilt tests carried out for different positions
764 of specimen 1, together with the theoretically computed angle of instability against sliding
765 (always the basic friction angle) and toppling (according to Eq. 2). The more prone
766 mechanism shows the lower angle of both computed, highlighted in bold in the figure.

767

768 **Figure 5** (a) tilt-test example; (b) 3D printer *BCN Sigma 3D* used; (c) printed concave
769 bases; (d) location of centres of gravity for force application in the different parts of the
770 rock element for computing factor of safety against toppling.

771 **Figure 6** Comparison of the experimental (x-axis) and theoretical (y-axis) angle of sliding
772 ('x') and toppling (dots) for all tested specimens.

773

774 **Figure 7** (a) Three different views of the set used for this experiment (shown in the
775 photo); (b) evolution of the left view of a tilt test in three positions (initial horizontal
776 position, after some tilting and at the critical case) indicating the projection on the tilting
777 plane of the base of the sample and that of the centre of gravity of the set. Remark
778 instability occurs when the projection of the weight attains the border of the base.

779

780 **Figure 8** Factor of safety of a single block with sharp edges (a) and rounded edges (b).

781

782 **Figure 9** Representative chart for three levels of the factor of safety (1, 1.2 and 1.5)
783 against toppling, for increasing rounding of edges (ρ from 0 to 1) and dip angle varying
784 from 0 to 60°.

785

786 **Figure 10** General view of the *Pena do Equilibrio* ('Equilibrium Stone').

787

788 **Figure 11** Different views of the boulder under study from aerial photography: West (a),
789 North (b), South (c) and top view (d). Note control points on photos (b) and (c).

790

791 **Figure 12** (a) Realistic view of the 3D point cloud with *CloudCompare*; (b) isolation of
792 3D point cloud of the boulder; (c) detail of a horizontal projection (top view) of the 3D
793 point cloud, including the polyline corresponding to the edge of the contact area.

794

795 **Figure 13** Illustrative screenshot from *CloudCompare* showing the forces involved on
796 the stability analysis against sliding and toppling for the boulder under study and
797 approximate location of the *cog*. The coordinate system is also provided.

798

799

800 **Figure 14** Projection on the contact plane of the *cog* and normal component of the weight
801 (W cosα)' for estimating safety factor against toppling.

802

803 **Figure 15** (a) Screenshot of the *BCN3D Cura* software to manage 3D printing; (b) top
804 and (c) bottom views of the printed boulder; (d) replica during one of the tilt-tests
805 performed.

806

807

808 **TABLE HEADINGS**

809

810 **Table 1** Experimental (β_i) and theoretical ($\beta_{theoretical}$) instability tilt angle for all specimens
811 with different positions tilted in laboratory until sliding (S) or toppling (T) failure occurs.
812 The different positions are illustrated in Figure 4 for specimen 1 and explained in the text.
813 $\beta_{toppling}$ is the angle theoretically computed for toppling instability. $\beta_{theoretical}$ is the lower
814 value between $\beta_{toppling}$ and friction angle (31±2º), theoretically indicating the angle at
815 which instability is expected. β_{mean} is the average of the observed experimental tilt tests
816 (β_1, β_2 and β_3). Error refers to the difference between the mean experimental angle
817 observed (β_{mean}) and the theoretical angle expected ($\beta_{theoretical}$).

818

819 **Table 2.** Geometrical parameters as recovered from 3D point cloud processing.

820

821 **Table 3**. Geomechanical parameters measured in joints.

822

823

824 **Table 4.** Results for the critical angle of toppling, analysed by means of tilt-test carried
825 out with the boulder replica.

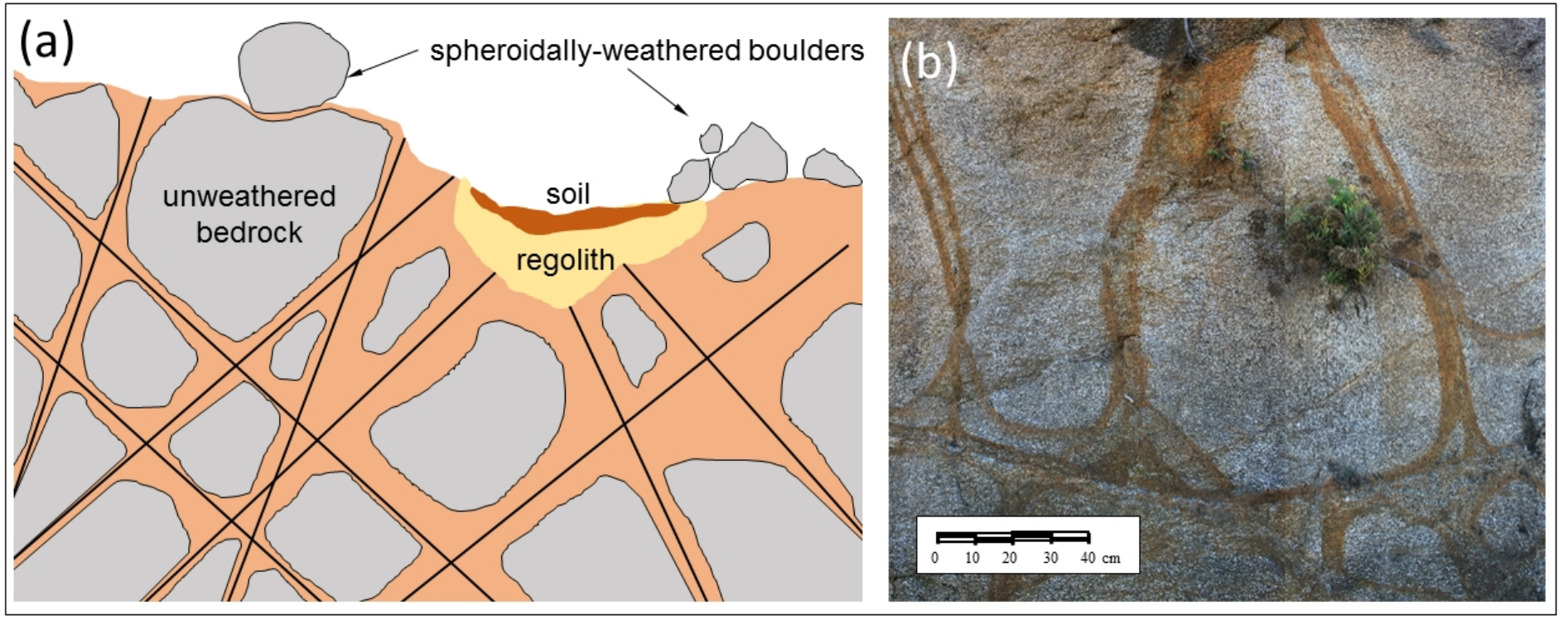
(a)
spheroidally-weathered boulders
unweathered
bedrock
soil
regolith
(b)
0 10 20 30 40 cm

(a)

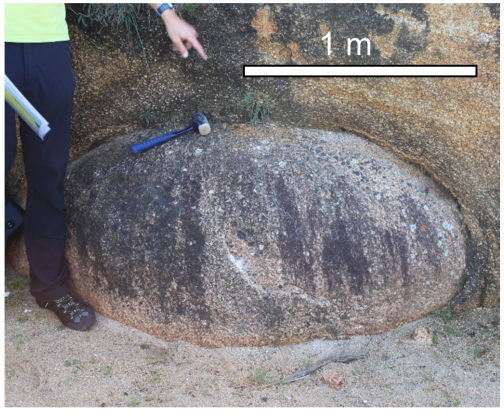

Sanxenxo, Galicia, Spain

(b)

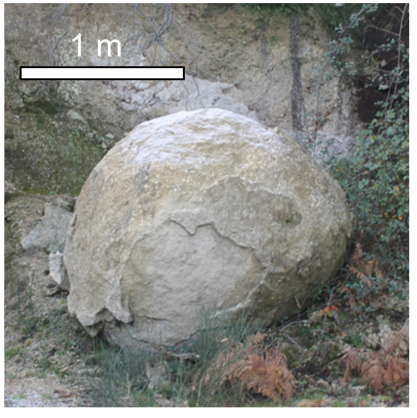

Coura, Minho, Portugal

(c)

Pontеareas, Galicia, Spain

(d)

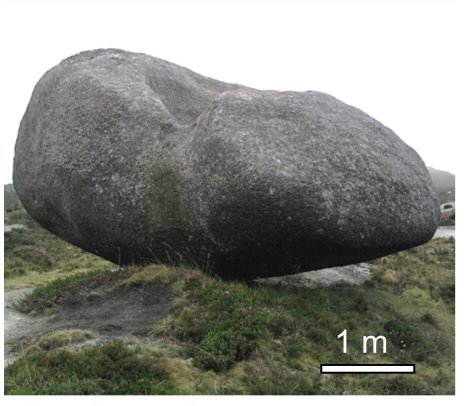

Alfoz, Galicia, Spain

(e)

Outeiro de Rei, Galicia, Spain

(f)

Serra de Arga, Minho, Portugal

(g)

Traba, Laxe, Galicia, Spain

(h)

Monte Pindo, Galicia, Spain

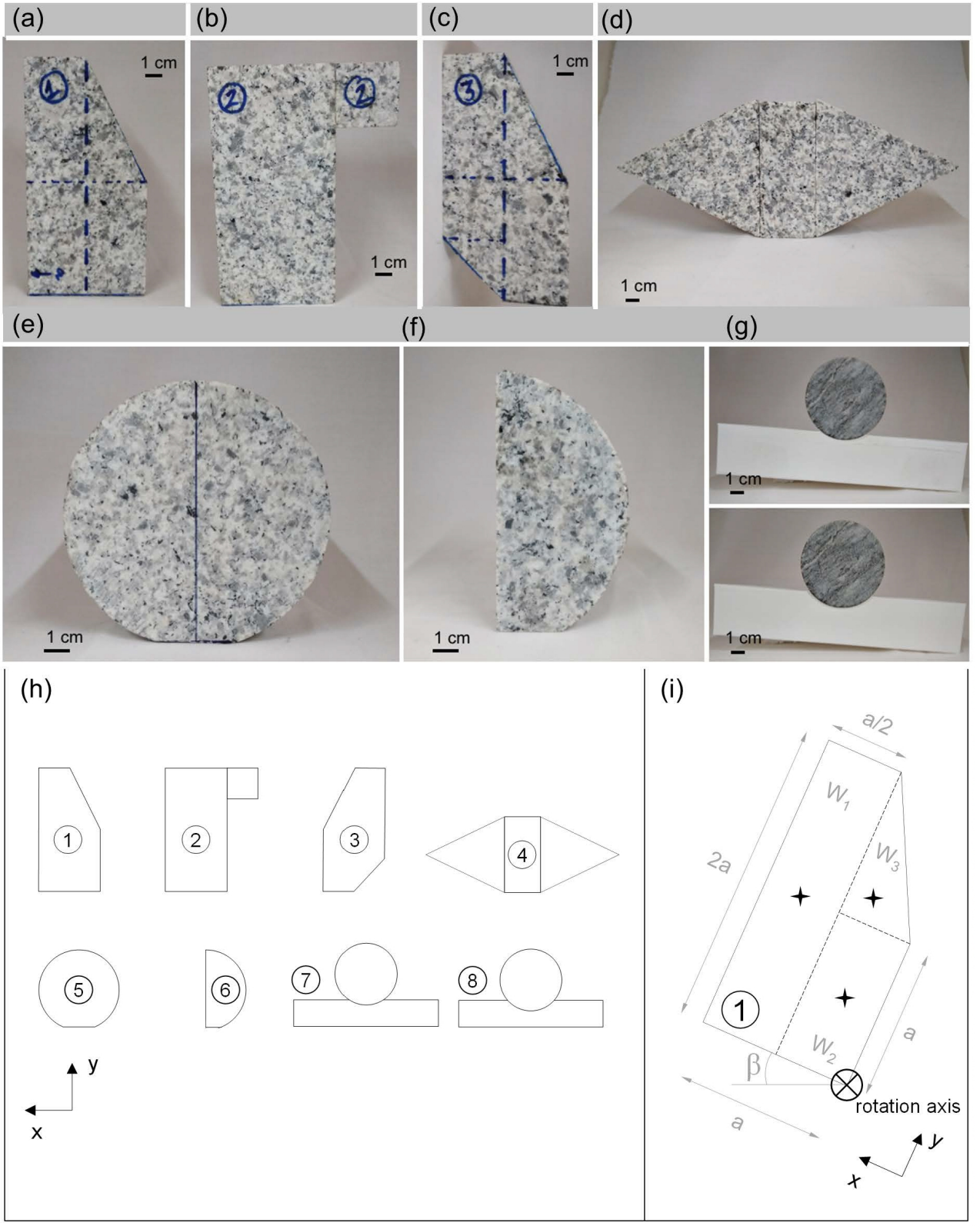
(a)
(b)
(c)
(d)
1 cm
(e)
(f)
(g)
(h)
1
2
3
4
5
6
7
8
y
x
(i)
a/2
2a
W_1
W_3
W_2
a
β
rotation axis
y
x

SIDE a

1-a1

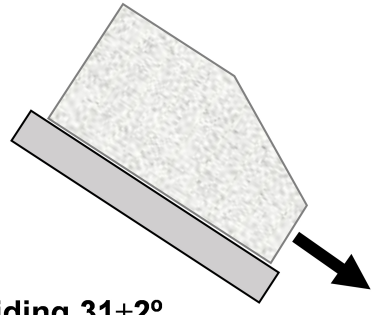

Sliding 31±2º
Toppling 67.5º

1-a2

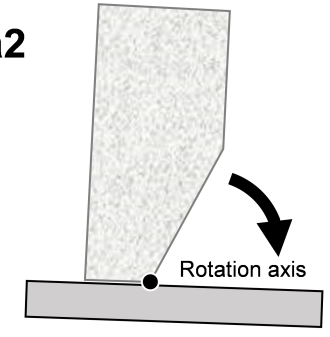

Sliding 31± 2º
Toppling 2.5º

1-a3

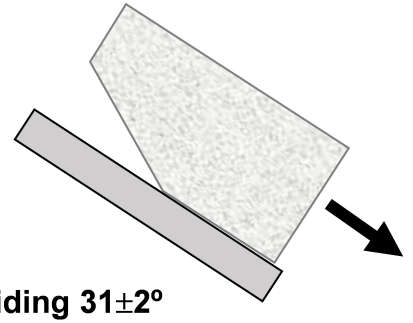

Sliding 31±2º
Toppling 58.8º

1-a4

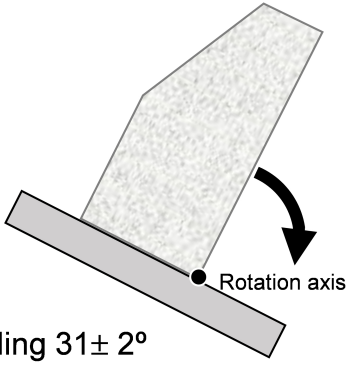

Sliding 31± 2º
Toppling 26.6º

SIDE b

1-b1

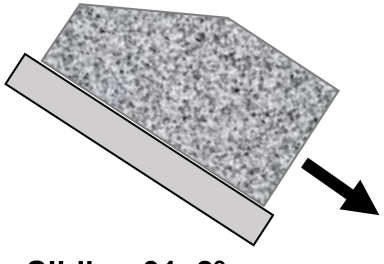

Sliding 31±2º
Toppling 56.7º

1-b2

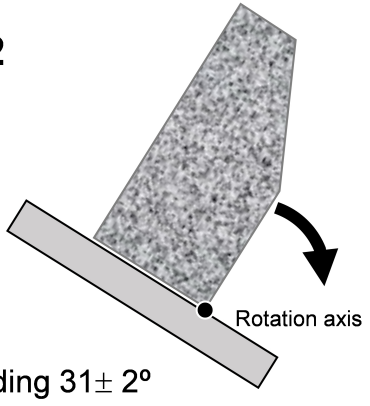

Sliding 31± 2º
Toppling 31.4º

1-b3

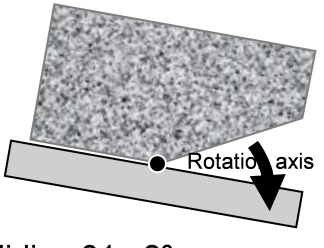

Sliding 31± 2º
Toppling 9.9º

1-b4

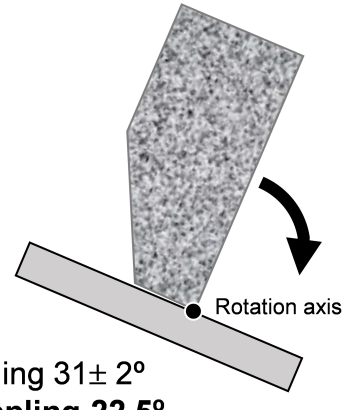

Sliding 31± 2º
Toppling 22.5º

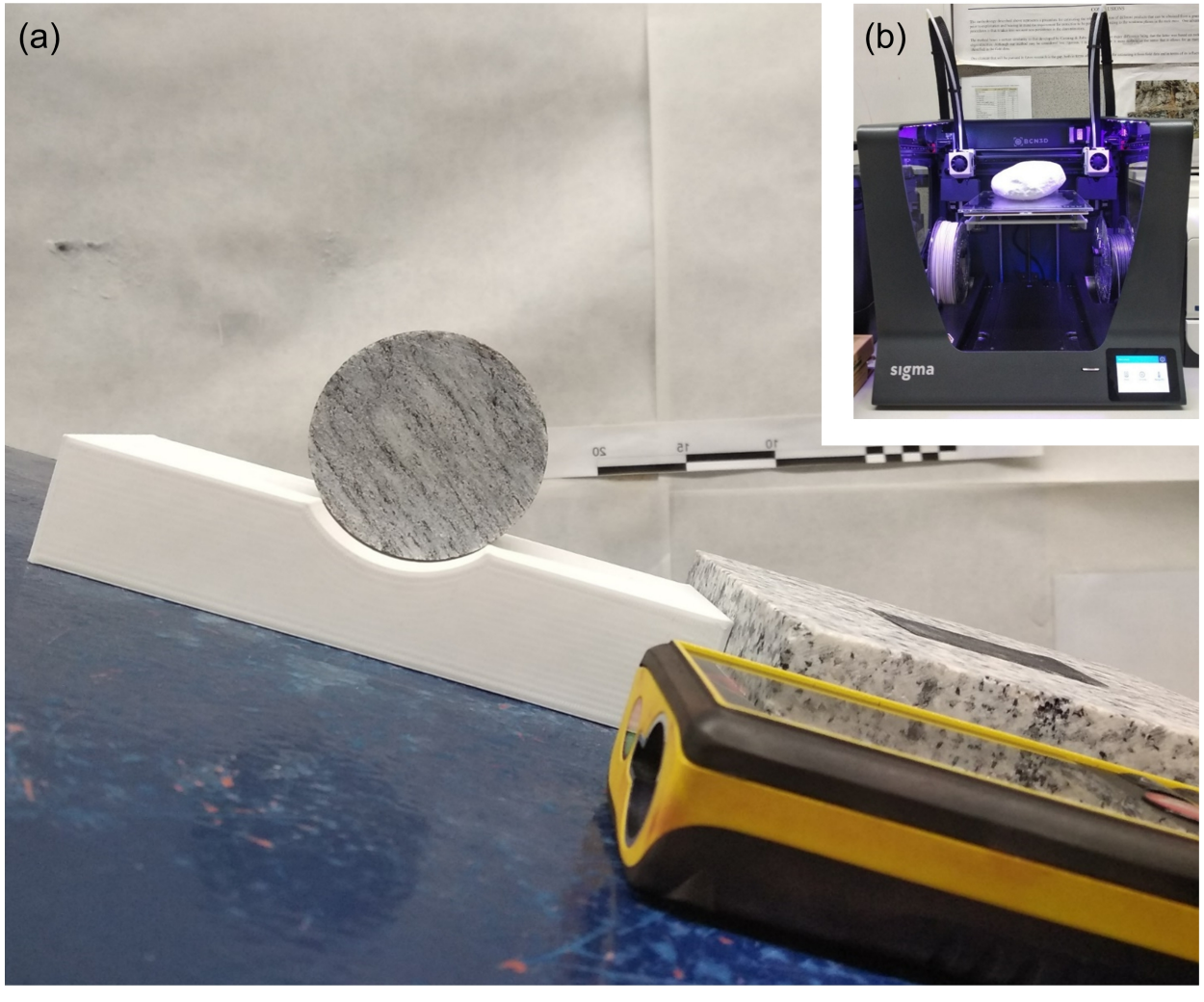
(a)

(b)
sigma

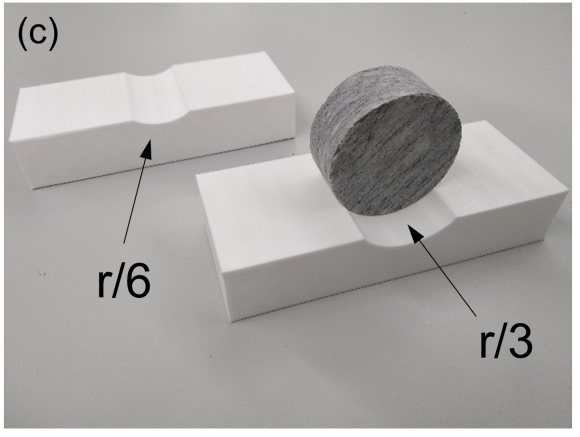
(c)
r/6
r/3

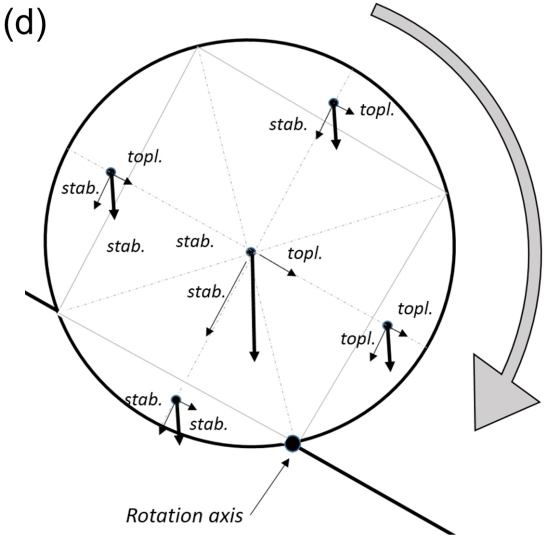
(d)
stab.
topl.
topl.
stab.
stab.
stab.
topl.
stab.
topl.
topl.
stab.
stab.
Rotation axis

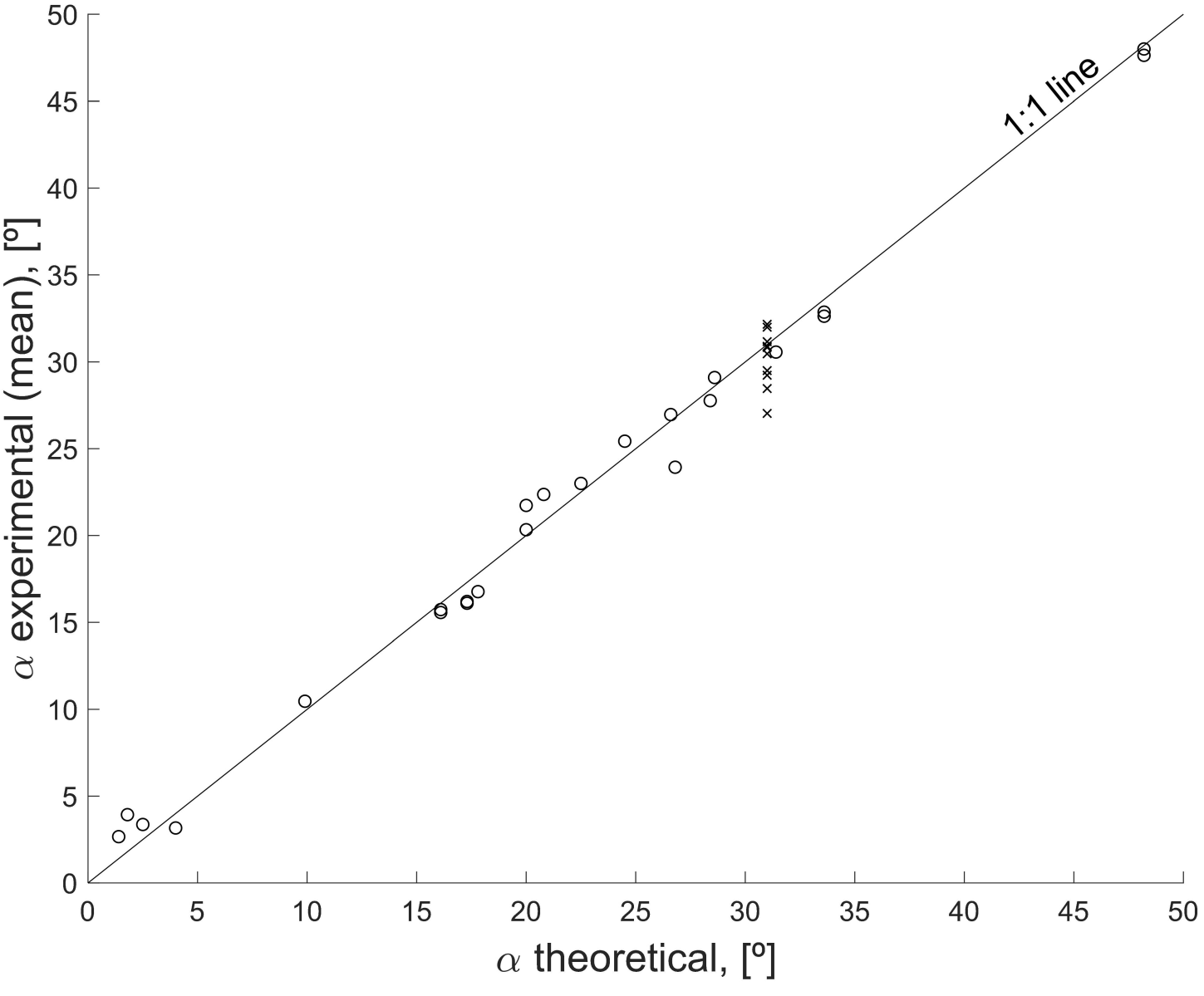
1:1 line
α experimental (mean), [º]
α theoretical, [º]
0
5
10
15
20
25
30
35
40
45
50

(a)

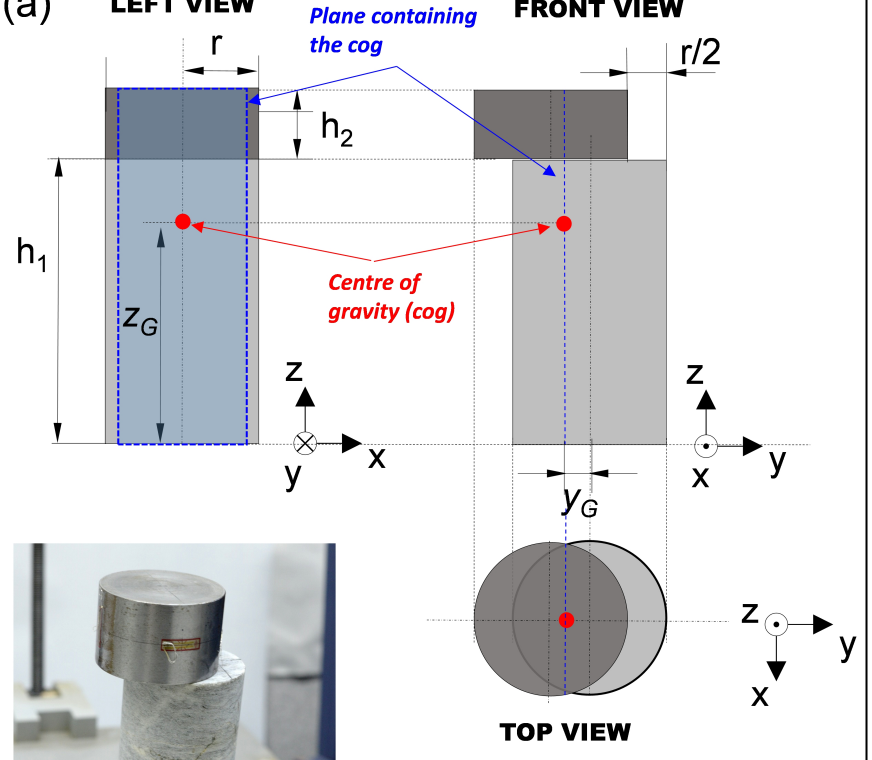

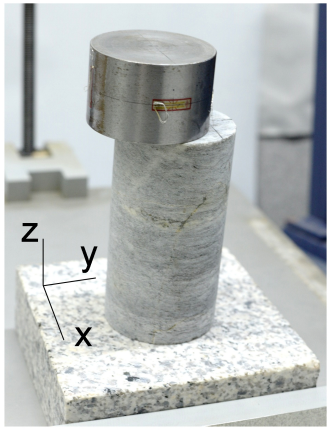

$$z_G = \frac{h_1/2\,(\pi r^2 h_1 \rho_1) + \left(h_1 + h_2/2\right)(\pi r^2 h_2 \rho_2)}{(\pi r^2 h_1 \rho_1) + (\pi r^2 h_2 \rho_2)} =$$

$$y_G = \frac{0 \cdot (\pi r^2 h_1 \rho_1) + 1/2\, r \cdot (\pi r^2 h_2 \rho_2)}{(\pi r^2 h_1 \rho_1) + (\pi r^2 h_2 \rho_2)} =$$

(b)

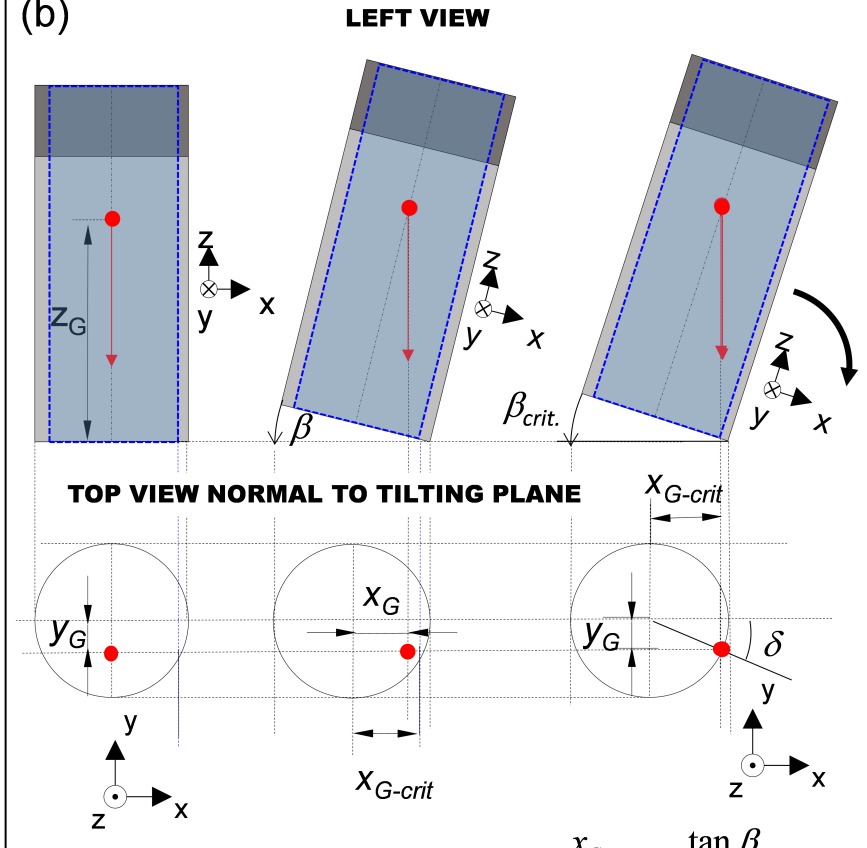

$$x_G = z_G \cdot \tan\beta$$

$$x_{G-crit} = \sqrt{r^2 - y_G^2} = z_G \cdot \tan\beta_{crit}$$

$$FoS = \frac{x_{G-crit}}{x_G} = \frac{\tan\beta_{crit}}{\tan\beta}$$

$$\delta = \tan^{-1}\left(y_G / x_{G-crit}\right)$$

(a) SHARP-EDGE BLOCK

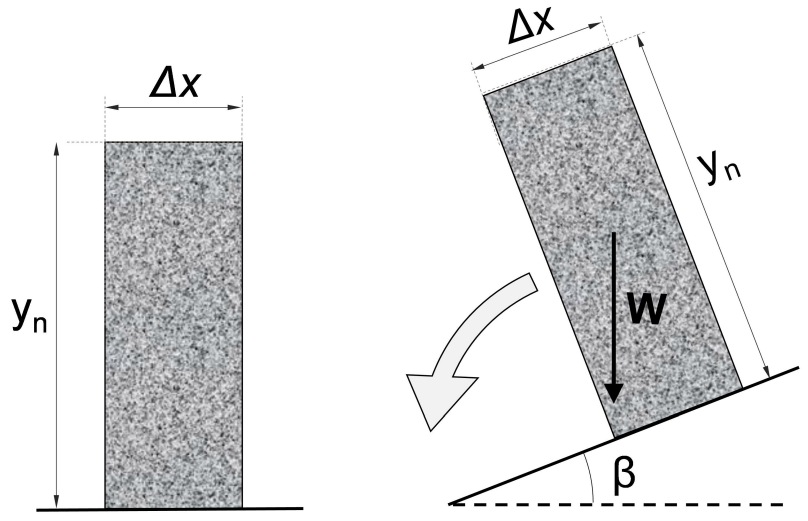

$$FoS = \frac{M_{stab.}}{M_{overt.}} = \frac{W \cos\beta \dfrac{\Delta x}{2}}{W \sin\beta \dfrac{y_n}{2}} = \tan^{-1}\beta \frac{\Delta x}{y_n}$$

(b) ROUNDED-EDGE BLOCK

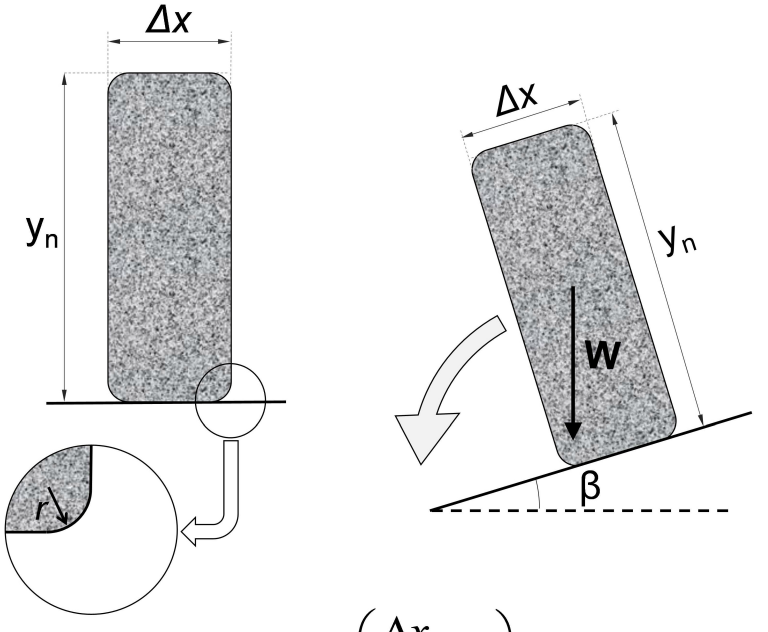

$$FoS = \frac{M_{stab.}}{M_{overt.}} = \frac{W \cos\beta \left(\dfrac{\Delta x}{2} - r \right)}{W \sin\beta \dfrac{y_n}{2}} = \tan^{-1}\beta \frac{\Delta x - 2r}{y_n}$$

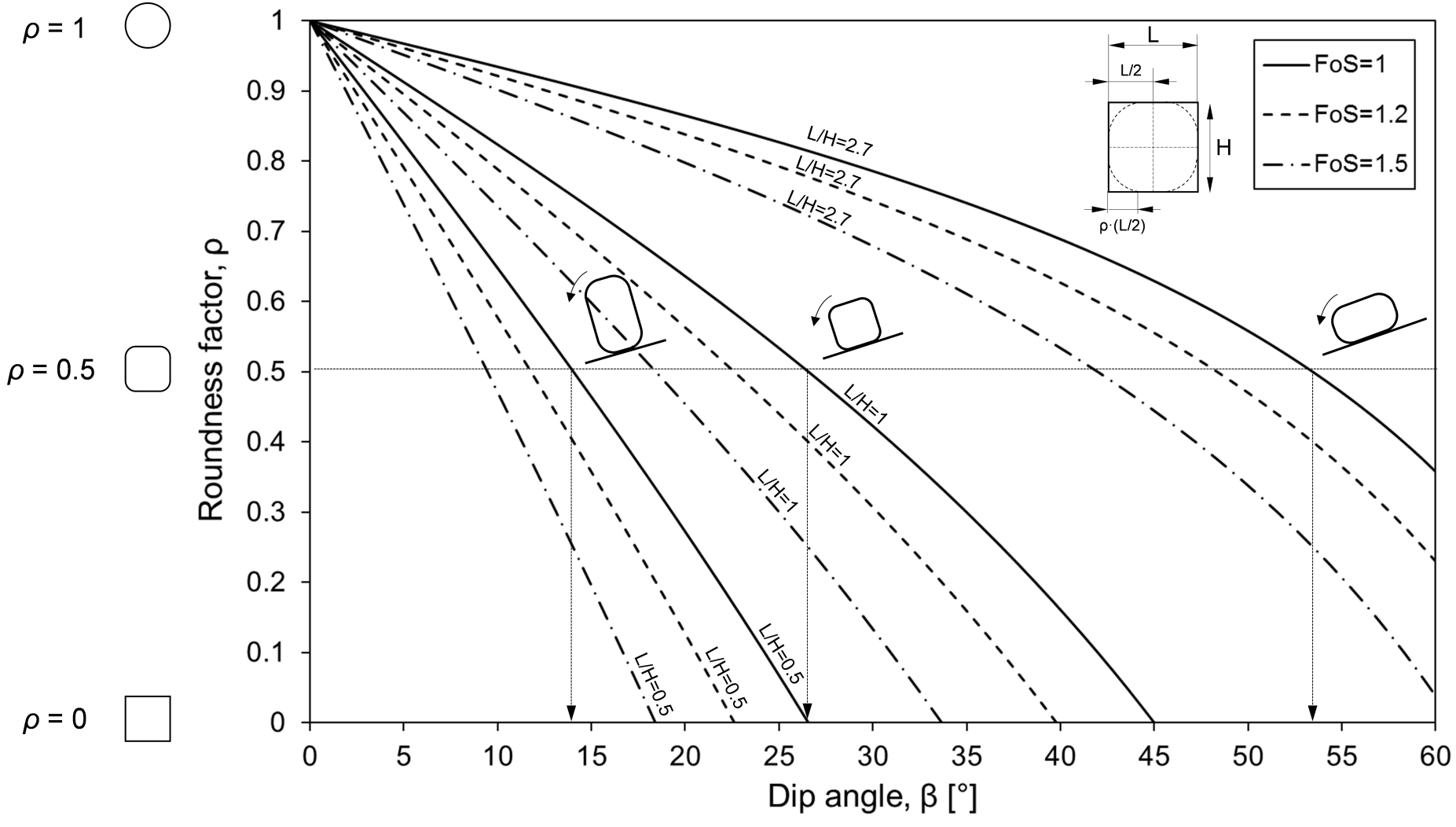
ρ = 1
ρ = 0.5
ρ = 0
Roundness factor, ρ
Dip angle, β [°]
0
0.1
0.2
0.3
0.4
0.5
0.6
0.7
0.8
0.9
1
0
5
10
15
20
25
30
35
40
45
50
55
60
L/H=2.7
L/H=2.7
L/H=2.7
L/H=1
L/H=1
L/H=1
L/H=0.5
L/H=0.5
L/H=0.5
L
L/2
H
ρ·(L/2)
FoS=1
FoS=1.2
FoS=1.5

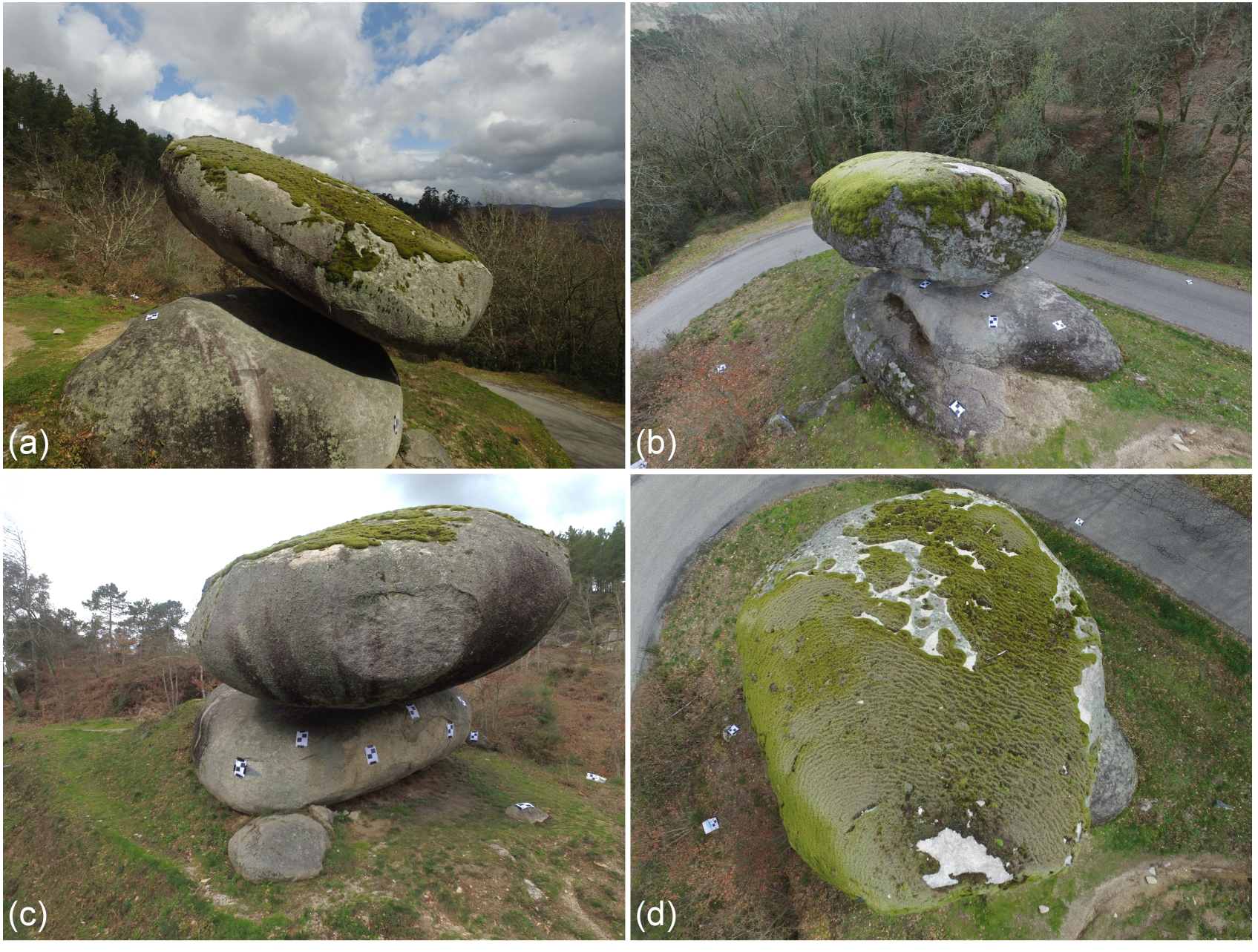
(a)
(b)
(c)
(d)

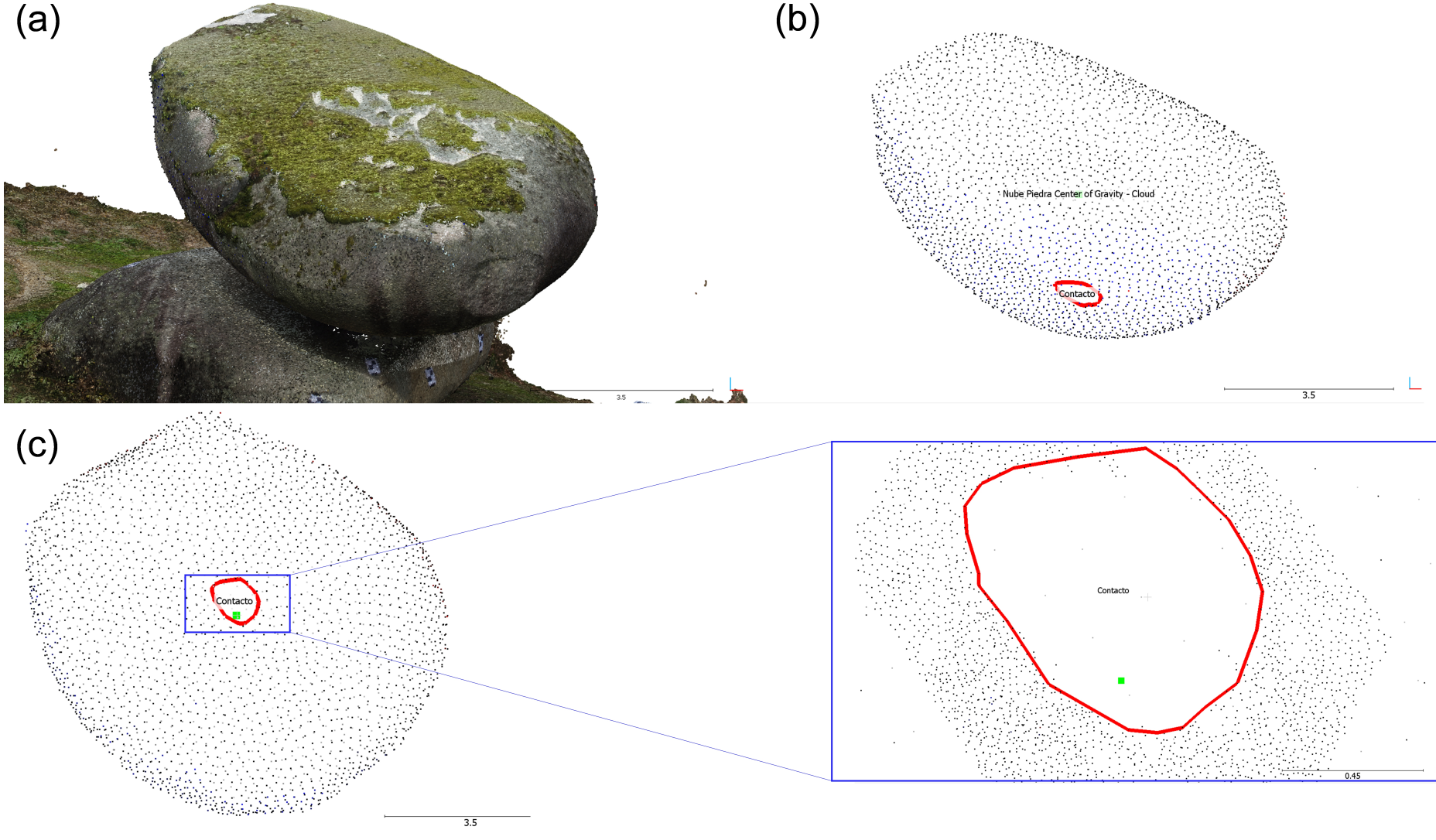
(a)
3.5
(b)
Nube Piedra Center of Gravity - Cloud
Contacto
3.5
(c)
Contacto
3.5
Contacto
0.45

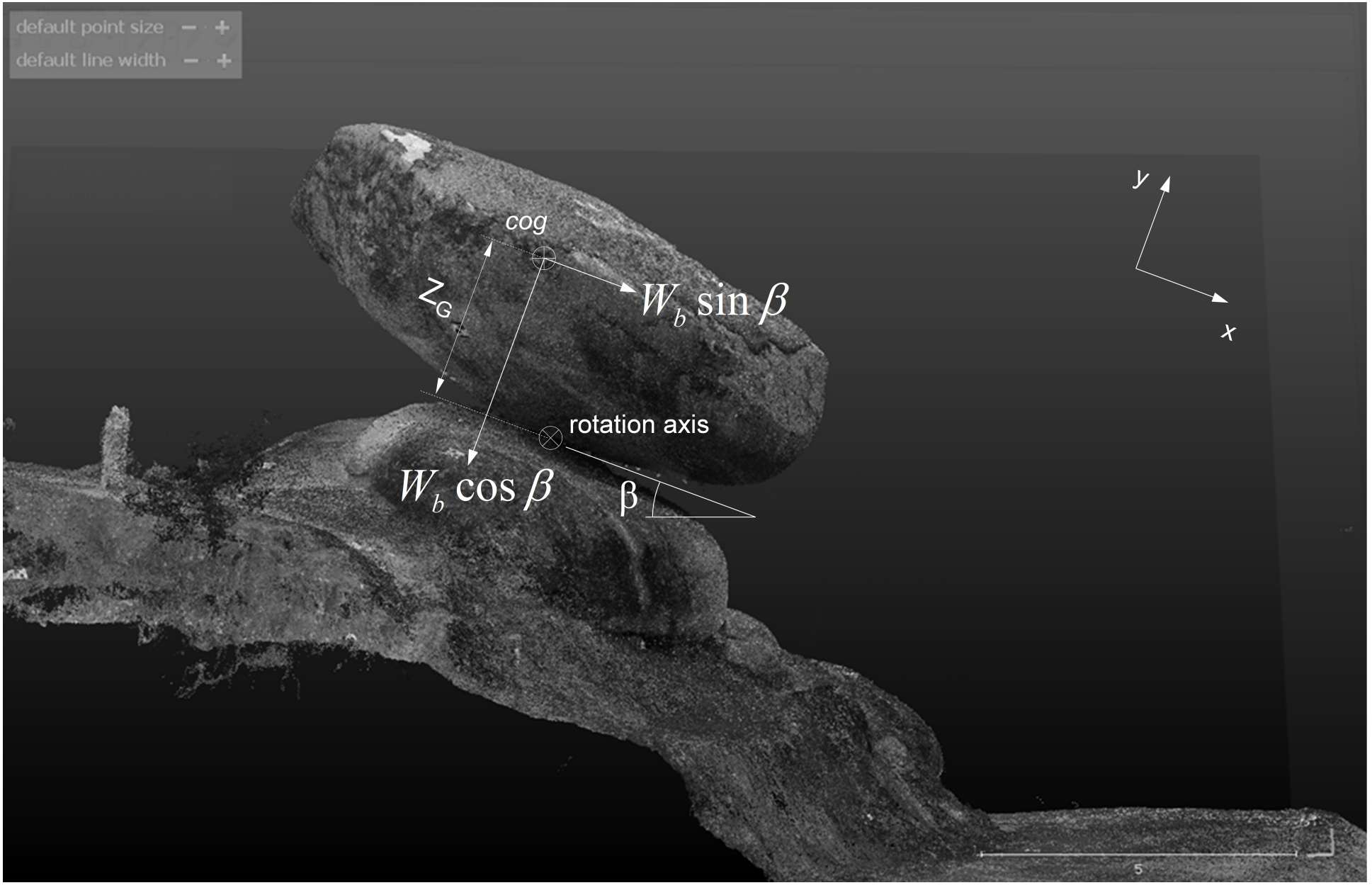
default point size
default line width
cog
z_G
$W_b \sin\beta$
rotation axis
$W_b \cos\beta$
β
y
x

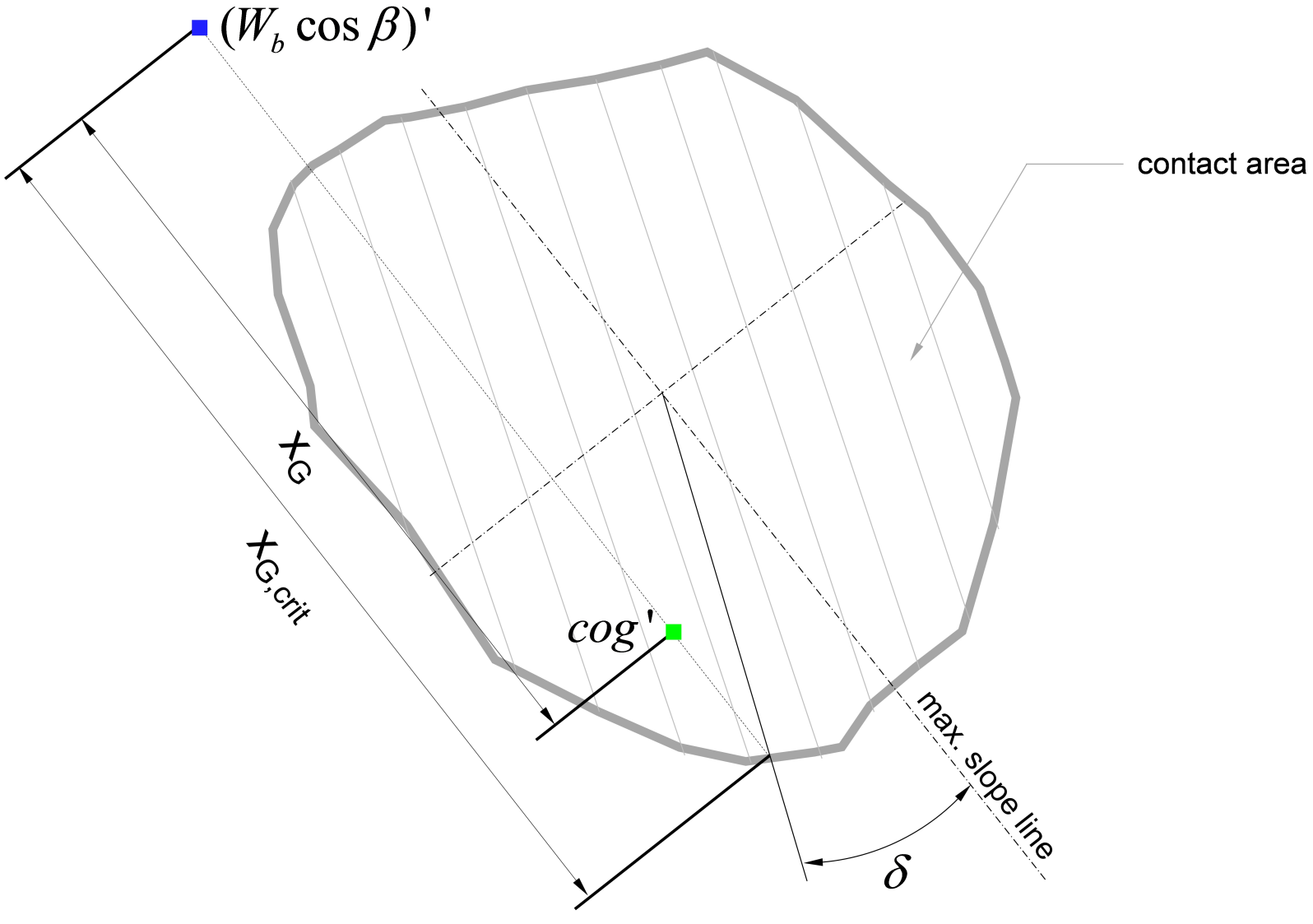
$(W_b \cos \beta)'$
contact area
x_G
$x_{G,crit}$
cog'
max. slope line
δ
0.5 m

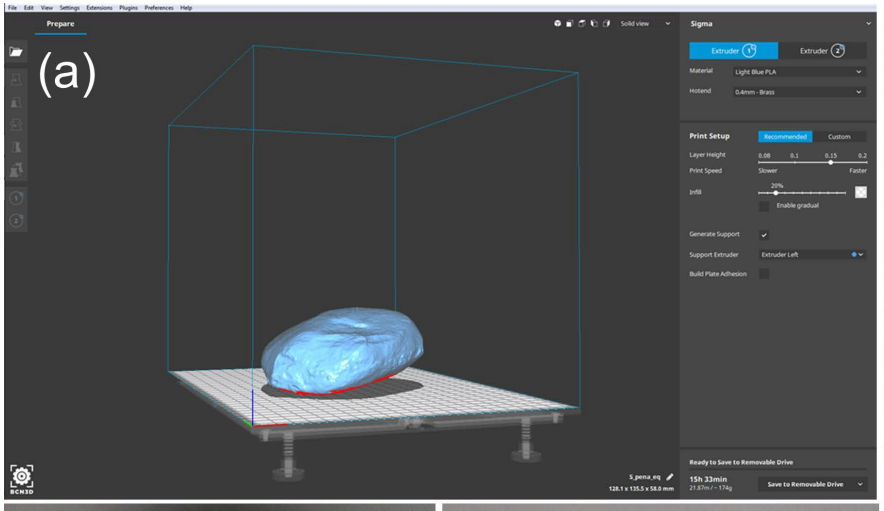
(a)
Prepare
Solid view
Sigma
Extruder 1
Extruder 2
Material
Light Blue PLA
Hotend
0.4mm - Brass
Print Setup
Recommended
Custom
Layer Height
Print Speed
Slower
Faster
Infill
20%
Enable gradual
Generate Support
Support Extruder
Extruder Left
Build Plate Adhesion
Ready to Save to Removable Drive
15h 33min
21.87m / ~ 174g
Save to Removable Drive
S_pena_eq
128.1 x 135.5 x 58.0 mm
BCN3D

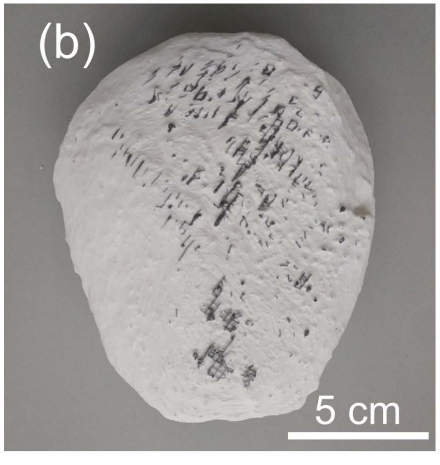
(b)
5 cm

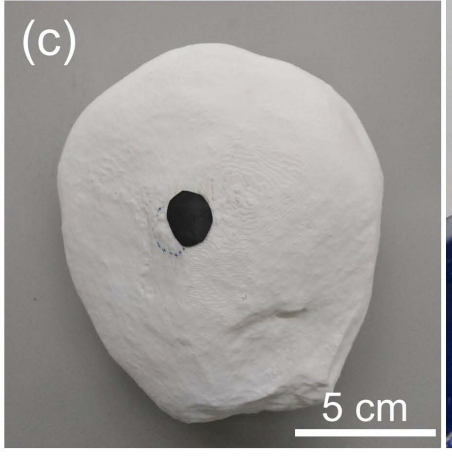
(c)
5 cm

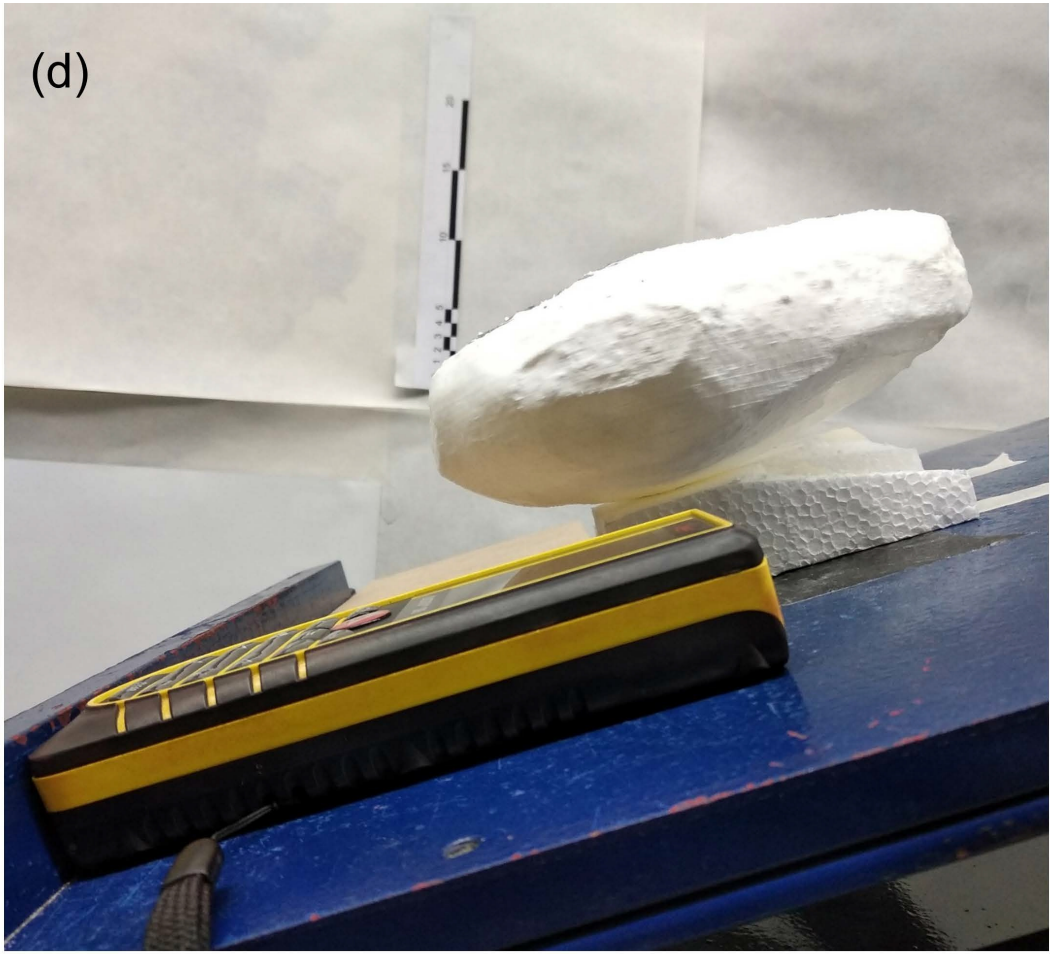
(d)

Table 1 Experimental (β_i) and theoretical ($\beta_{theoretical}$) instability tilt angle for all specimens with different positions tilted in laboratory until sliding (S) or toppling (T) failure occurs. The different positions are illustrated in Figure 4 for specimen 1 and explained in the text. $\beta_{toppling}$ is the angle theoretically computed for toppling instability. $\beta_{theoretical}$ is the lower value between $\beta_{toppling}$ and friction angle (31±2º), theoretically indicating the angle at which instability is expected. β_{mean} is the average of the observed experimental tilt tests (β_1, β_2 and β_3). Error refers to the difference between the mean experimental angle observed (β_{mean}) and the theoretical angle expected ($\beta_{theoretical}$).

Specimen	Position	$\beta_{toppling}$	$\beta_{theoretical}$	S/T	β_1	β_2	β_3	β_{mean}	error
1	a1	67.5	31±2	S	33.7	30.2	29.6	31.2	0.2
	a2	2.5	2.5	T	3.5	3.3	3.3	3.4	0.9
	a3	58.8	31±2	S	34.8	30.6	27.3	30.9	-0.1
	a4	26.6	26.6	T	27.4	27.2	26.3	27.0	0.4
	b1	56.7	31±2	S	33.0	31.5	28.0	30.8	-0.2
	b2	31.4	31±2	T	30.9	30.4	30.4	30.6	-0.4
	b3	9.9	9.9	T	10.8	10.4	10.2	10.5	0.6
	b4	22.5	22.5	T	22.9	23.1	23.0	23.0	0.5
2	a1	57.5	31±2	S	32.8	25.3	27.3	28.5	-2.5
	a2	45.0	31±2	S	34.2	31.2	30.6	32	1
	a3	28.4	28.4	T	27.8	27.8	27.7	27.8	-0.6
	b1	61.7	31±2	S	34.6	26.8	27.1	29.5	-1.5
	b2	32.6	31±2	S	32.3	32.1	32.1	32.2	1.2
	b3	20.8	20.8	T	22.7	22.1	22.3	22.4	1.6
3	a1	66.0	31±2	S	33.5	30.9	27.0	30.5	-0.5
	a2	1.4	1.4	T	2.60	2.70	2.70	2.70	1.3
	a3	61.4	31±2	S	29.0	25.6	26.5	27.0	-4
	a4	< 0	-	-	-	-	-	-	
	b1	45.0	31±2	S	30.4	27.2	30.1	29.2	-1.8
	b2	24.5	24.5	T	25.4	25.3	25.6	25.4	0.9
	b3	4	4	T	3.20	3.20	3.10	3.20	-0.8
	b4	28.6	28.6	T	29.1	29	29.2	29.1	0.5
4	a1	20.0	20.0	T	20.2	20.3	20.5	20.3	0.3
	a2	20.0	20.0	T	21.6	21.8	21.8	21.7	1.7
5	a1	16.1	16.1	T	15.6	15.6	15.5	15.6	-0.5
	a2	16.1	16.1	T	15.7	15.7	15.8	15.7	-0.4
6	a1	1.80	1.80	T	3.9	4.1	3.8	3.90	2.1
	a2	26.8	26.8	T	23.8	23.8	24.2	23.9	-2.9
7	a1	33.6	33.6	T	33.3	32.5	32.8	32.9	-0.7
	a2	33.6	33.6	T	32.7	32.6	32.6	32.6	-1.0
8	a1	48.2	48.2	T	47.3	48.3	48.4	48.0	-0.2
	a2	48.2	48.2	T	46.7	47.2	49.0	47.6	-0.6
Set rock + steel	Left r/2	17.3	31±2	T	16.5	15.9	16.2	16.2	-1.1
	Centred	17.8	31±2	T	16.9	16.9	16.5	16.8	-1.0
	Right r/2	17.3	31±2	T	16.1	15.8	16.4	16.1	-1.2

Table 2. Geometrical parameters as recovered from 3D point cloud processing.

Geometrical parameter	Units	Value
Volume, V_b	[m^3]	142.22
Centre of gravity, *cog*	x, y, z coordinates [m]	7.915, -2.854, 113.036
Theoretical contact area, A	[m^2]	0.61
Contact plane dip direction	[°]	163
Contact plane dip, β	[°]	27

Table 3. Geomechanical parameters measured in joints.

Parameter	Values	Mean	Standard deviation
Average Schmidt hammer rebounds (*r*) in surfaces	34.5, 51.2, 45.2 52, 47.2, 48, 44.5, 45.5	46	5.5
Average Schmidt hammer rebounds on fresh rock (*R*)	50, 52, 54, 48, 56	52	3.2
JRC	8, 6, 8, 12, 6, 10, 16, 10	11	3.8
JCS based on (*r*), [MPa]		112	30

Table 4. Results for the critical angle of toppling, analysed by means of tilt-test carried out with the boulder replica.

Test	1	2	3	4	5
β_{test} [°]	30.8	30.4	30.7	29.8	30.3